UNIVERSITY OF CALIFORNIA, SAN DIEGO

Theory and application of open quantum systems

A dissertation submitted in partial satisfaction of the
requirements for the degree
Doctor of Philosophy

in

Physics

by

Ching-Kit Chan

Committee in charge:

Professor Lu Jeu Sham, Chair
Professor Yeshaiahu Fainman
Professor Michael Fogler
Professor Shayan Mookherjea
Professor Oleg Shpyrko

2012

The dissertation of Ching-Kit Chan is approved, and it is acceptable in quality and form for publication on microfilm and electronically:

_____

_____

_____

_____

_____
Chair

University of California, San Diego

2012

DEDICATION

To Shenshen, and our parents.

TABLE OF CONTENTS

LIST OF FIGURES

ACKNOWLEDGEMENTS

I would like to start by expressing my deepest gratitude to my supervisor, Prof. Lu Sham, who brought me into this exciting and rapidly growing field of quantum information science three years ago. His comprehensive knowledge in both fundamental and applicable science stimulated and reshaped my basic understanding of physics. His outstanding insight also provided me a really different horizon to view and pursue scientific research in a unique manner. I learned from him how to achieve scientific breakthrough by keep questioning the fundamentals of science and going beyond any traditional paradigm that was thought to be completely understood. I really enjoyed the inspiring weekly meeting with Lu. In particular, I would like to thank Lu and Georgina for inviting me to their thanksgiving party each year, and many other invitations, making me feel like home in my PhD study.

I would like to thank Prof. Yeshaiahu Fainman, Prof. Michael Fogler, Prof. Shayan Mookherjea and Prof. Oleg Shpyrko for being my PhD committee members and asking inspiring questions. I would also like to thank our group members, Giuseppe Barbalinardo, Kilhyun Bang, Libo Chen, Shengnan Ji, Xiaofeng Shi, Tiamhock Tay, Yong Wang and Wen Yang, who have helped me a lot about work and life in the past years. I learned a lot of interesting new ideas through many inspiring scientific discussion with them. I am also grateful to Prof. Congjun Wu for his guidance during my first PhD year at UCSD.

Last but not least, I want to express my grand gratefulness to my wife, Shenshen, and our parents, who continuously support, encourage and give surprises during my PhD in US. They make me feel I am never alone. If I get lost in science, they will always accompany with me and help me pass through.

Chapter 2, in part, is a reprint of the material as it appears in Ching-Kit Chan and L. J. Sham, "Precision of electromagnetic control of a quantum system", Physical Review A **84**, 032116 (2011). The dissertation author was the first author of the paper and the co-author in this publication directed, supervised, and coworked on the research which forms the basis of this chapter.

Chapter 3, in part, is a reprint of the material as it appears in Ching-Kit

Chan and L. J. Sham, "Quantum correlation of an optically controlled quantum system", Journal of the Optical Society of America B, Feature issue,**29**, A25, (2012). The dissertation author was the first author of the paper and the co-author in this publication directed, supervised, and co-worked on the research which forms the basis of this chapter.

Chapter 4, in part, is a reprint of the material as it appears in Ching-Kit Chan and L. J. Sham, "Robust distant-entanglement generation using coherent multiphoton scattering", under review of Physical Review Letter. The dissertation author was the first author of the paper and the co-author in this publication directed, supervised, and co-worked on the research which forms the basis of this chapter.

VITA

2002-2005	Bachelor of Science in Physics, First class honors, Hong Kong University of Science and Technology, Hong Kong
2005-2007	Master of Philosophy in Physics, Hong Kong University of Science and Technology, Hong Kong
2007-2008	Teaching and Research Assistant, Department of Physics, Columbia University, New York, USA
2008-2012	Research Assistant, Department of Physics, University of California, San Diego, USA
2012	Doctor of Philosophy in Physics, University of California, San Diego, USA

PUBLICATIONS

Ching-Kit Chan and L. J. Sham, "Robust distant-entanglement generation using coherent multiphoton scattering", under review of Physical Review Letter.

Ching-Kit Chan and L. J. Sham, "Quantum correlation of an optically controlled quantum system", Journal of the Optical Society of America B, Feature issue, **29**, A25, (2012).

Ching-Kit Chan and L. J. Sham, "Precision of electromagnetic control of a quantum system", Physical Review A **84**, 032116 (2011).

ABSTRACT OF THE DISSERTATION

Theory and application of open quantum systems

by

Ching-Kit Chan

Doctor of Philosophy in Physics

University of California, San Diego, 2012

Professor Lu Jeu Sham, Chair

Quantum information science is a rapidly growing research area for that it provides new insights to the fundamentals of quantum mechanics and offers a platform for the architecture of novel quantum technologies. The successfulness and practicality of this important scientific field rely on the controllability of a quantum system subject to a realistic noisy environment. The environment always leads to unintended dynamics of the system, and thus destroys its coherence and limits its applications. It is therefore important to understand these decoherence mechanisms from first principles, in order to minimize, or even remove, its adverse effect on the quantum system. The study of this open quantum system problem is usually based on some effective paradigms, where the environment is assumed to be "large", such that it can affect the quantum system without any

back action. However, due to the demand for a high precision in quantum computation, such an approximate framework becomes questionable. We provide a new theoretical approach to treat this type of open quantum system problem, including the correlated dynamics between the system and the environment, by using a diagrammatic technique in the same spirit as the Keldysh non-equilibrium Green's function. In this formalism, both the environment and the photonic control are quantized. The dynamics of the system can be evaluated accurately for a time scale of small decoherence, but arbitrary quantum control, relevant to the need for quantum technologies. This offers a way of precise quantum noise calculations. We find how fundamental quantum correlations between the quantum control and quantum environment can arise, and are missing in the existing Master equation approximations. On the other hand, the study of the environment not only provides a better understanding of the decoherence, it also allows applicable designs of quantum operations between different qubit systems. In particular, we engineer a new protocol to entangle two qubits at a distance by projection measurements of their environments, the resonance fluorescence photons. We find exceptional improvements on the probability of success and the rate of entanglement based on the multiphoton environment approach, in comparison with the existing single photon entanglement scheme.

Chapter 1

Introduction

1.1 The importance of a precise study of quantum noise

Since the proposal of quantum computing by Feynman in 1982 [1], tremendous amount of research opportunity has been opened along this direction due to its broad impact on various subjects, from the fundamental understanding of quantum mechanics to the exponential speedup of computational power. One of the most famous applications is the Shor's algorithm [2], by which a quantum computer can factorize an N-digit number in a polynomial time scale $\sim N^2 \log N \log(\log N)$, being much faster than the best known classical computational time $\sim \exp(N^{1/3})$. Such an exponential boost of computational speed has been shown to be important to quantum cryptography and quantum information processing.

In the last decade, an enormous amount of effort has been put into this research field by attempts to construct a realistic quantum computer based on various quantum bit (qubit) protocols. They include the polarization photon qubits, solid state qubits based on electrons in quantum dot (QD) systems, superconducting qubits, trapped ions, diamond based nitrogen-vacancy (NV) qubits, etc. Tremendous amounts of successes have been demonstrated in the controllability of single qubit systems. More recently, small scale quantum manipulations of qubits have been realized in experiments including two-qubit algorithm [3], long distance

quantum entanglement [4], quantum teleportation of photons [5], etc.

Yet, a realistically sizable quantum computer has not been manufactured because of the scalability problem. This can be explained from the view of quantum error correction. Unlike the classical computer, a single qubit cannot be measured for possible errors during the operation as a measurement would collapse the wavefunction of the qubit. Also, a qubit cannot be cloned either because of the no-cloning theorem in quantum mechanics, making quantum error correction extremely difficult. The study of fault tolerant quantum computation has shown that an arbitrary long quantum computation is possible if the error of each quantum operation is less than certain threshold ϵ_0. Such an error threshold is as small as $\sim 10^{-4}$ [6] and is not reached by any present experiments (in fact, in existing experimental practice, the ability to even detect such a small error is very questionable). We are also questioning whether the theory has the accuracy to predict and thus help design physical processes, which can meet the stringent threshold requirement.

The main source of error of a qubit is the decoherence as a result of any correlated dynamics between the qubit and the surrounding environment. Examples include the spontaneous emission of photons due to the coupling between an electron qubit and the unavoidable electromagnetic vacuum, the hyperfine interaction between a spin qubit and an environment of 10^6 nuclear spins, phonon scattering due to thermal fluctuation, etc. These environmental noise limits the coherence of a qubit within certain fixed decoherence time. In order to optimize, or hopefully eliminate, the decoherence of a qubit system, a precise understanding of the decoherence mechanism is necessary. Therefore, an accurate theory to evaluate the decoherence and quantum noise of an open quantum system, that can match the high fidelity requirement by the fault tolerant quantum computation, is particularly important for scalable quantum technologies.

The study of a quantized control has the same importance to quantum information processing. A quantum control can be treated as a macrosystem that quantum mechanically couples to the qubits and can cause noise through back action. A suitable candidate of open quantum system should be able to quantize

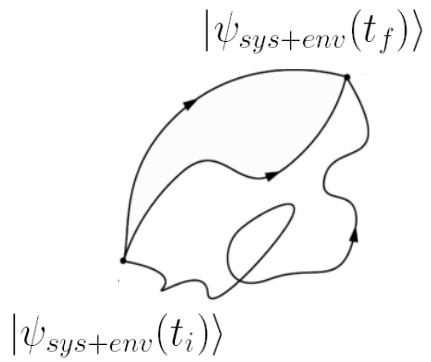

Figure 1.1: The influence-functional path-integral approach includes all possible trajectories of the total wavefunction of the quantum system and the environment from an initial time t_i to a final time t_f. While this method keeps track of all the quantum correlations of the total system, the influence functional is in general hard to compute due to the huge Hilbert space of the problem.

both the control and the environment on a equal footing. The joint correlation effects of the quantum control and the quantum environment form the main subject of this dissertation.

1.2 Various open quantum system theories

The first theoretical approach to open quantum system problems was based on the path integral approach by Feynman and Vernon [7]. The idea is to integrate out all possible quantum trajectories of an initial wavefunction that describes both the quantum system of interest and the environment as depicted in Fig. (1.1). The time evolution of the total wavefunction is governed by the underlying interaction Hamiltonian between of the system and the environment. Since we are only concerned about the system, the environmental degrees of freedom of the total density matrix is traced out at some final time, resulting in a reduced density matrix of the system. They relate the initial ($\rho_{sys}(t_i)$) and final ($\rho_{sys}(t_f)$) density matrix by the influence-functional $J(x, t_f; x', t_i)$:

$$\rho_{sys}(x, t_f) = \int dx' J(x, t_f; x', t_i) \rho_{sys}(x', t_i), \tag{1.1}$$

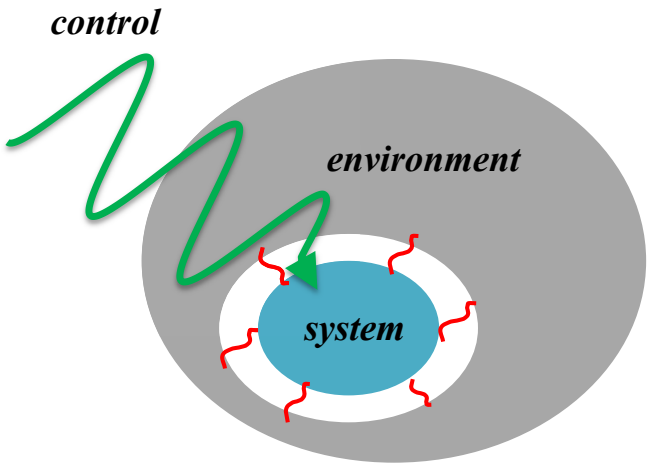

Figure 1.2: In the Master equation framework, an open quantum system interacts weakly with a large environment. The environment is treated as a reservoir and its density matrix is assumed to be unaffected by the quantum system. The control agent is usually described by some external parameters and is also assumed to be not influenced by the quantum system.

This approach is formally exact and all the quantum correlations between the system and environment are maintained in the influence-functional. However, in general, it is a difficult task to evaluate this influence functional as there are usually too many possible paths to be integrated out. An approximate treatment to this problem is needed.

One of the successful approximate framework to this quantum mechanical problem is based on the Master equation formalism (see for example [8, 9]). The physical picture, as shown in Fig. (1.2), is that an open quantum system is assumed to interact weakly with a "sufficiently large" environment, so that the effect of the environment is approximated as an effective potential that dissipates the small quantum system. This relies on a priori assumption that the quantum system has no back action to the environment and the density matrix of the environment can be approximated as being time-independent. Also, the control agent that drives the quantum system, say laser, is treated as some external parameter on the system, and again experiences no back action from the quantum system. Based on these criteria, we can write down an effective Master equation that governs the flow of

the reduced density matrix of the system:

$$\frac{d}{dt}\rho_{sys}(t) = -i[H_C(t), \rho_{sys}(t)] + \int_0^t dt' \hat{K}(t-t')\rho_{sys}(t'), \tag{1.2}$$

where $H_C(t)$ is a time-dependent external control Hamiltonian and $\hat{K}$ is a suitably chosen superoperator responsible for the dissipation of the environment. In comparison with the path integral approach, the many path nature of this quantum mechanical problem disappears under the above construction.

The Master equation formalism has been widely utilized in different areas of research due to its straightforwardness and the fact that many traditional problems satisfy the assumptions described above. Nevertheless, in the context of quantum information science, where high accuracy standard is demanded, it is necessary to carefully reexamine the Master equation formalism. In particular, the following fundamental questions are essential to be addressed:

- What is the error bound of the approximate theory? How does it compare with the error threshold requirement by fault tolerant quantum computation?
- What is the physical condition(s) for any stochastic assumption?
- How will the theory be modified, if the system interacts strongly with the environment?
- How can we go beyond the classical treatment of the control agent and include back action from the system to the quantum control?
- Is there any quantum correlation among the system, the quantum environment and the quantum control?

Bearing the above questions in mind, we have developed a new theoretical framework to go beyond the existing Master equation paradigm. This theoretical approach is based on a diagrammatic formulation of the open quantum system, in the same spirit as the Keldysh non-equilibrium Green's function used in condensed matter physics. We find that diagrammatic approach is in fact very suitable to

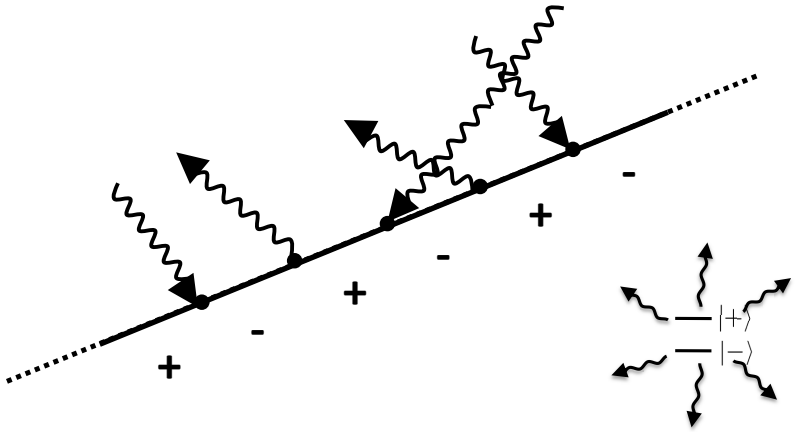

Figure 1.3: In the diagrammatic approach, the open quantum system has a small trajectory space. The evolution of the total system is thus described by summing different diagrams corresponding to different paths of the environment. Partial summations can be carried out systematically under this construction. This figure shows a two state system interacting with a photonic environment, in which the two states are flipped back and forth by the photons.

treat open quantum system, owing to the fact that the system has a small Hilbert space (see Fig. (1.3)). This approach permits a computationally easy way of partial summations of the diagrams and leads to a highly accurate calculation of the decoherence of the open quantum system, where both the environment and the control are quantized.

In chapter 2, we provide a systematic study of the problem of a two level system interacting with a non-Markovian photonic environment. Based on some basic examples, we illustrate how this new diagrammatic approach can lead to a higher precision than existing Master equation solutions. In chapter 3, we apply this method to the problem with a quantum photon control. Fundamental and interesting quantum correlations among the system, the control and the environment are found.

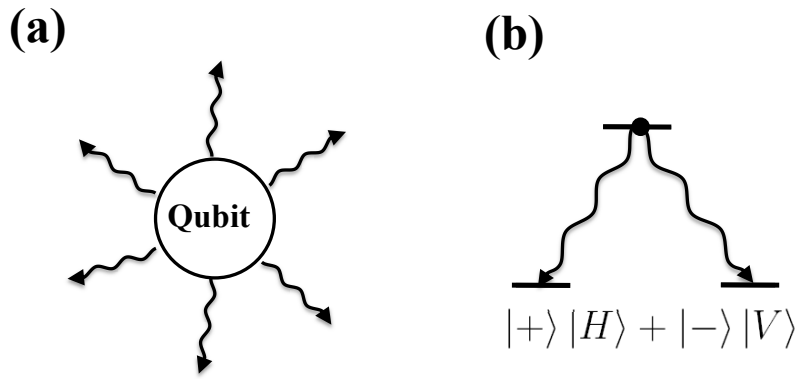

Figure 1.4: Two sides of an open quantum system coupling to the same photonic environment. (a) An initially excited quantum system can spontaneously emit a photon and decay to the ground state. This is simply decoherence of the qubit as we trace over the emitted photons. (b) The same qubit system can in fact be entangled with the emitted photons, if we have a complete knowledge of the internal qubit-photon wavefunction. The figure shows a simple example of how a qubit entangle with two different polarization modes $|H(V)\rangle$ of the emitted photon.

1.3 Application of the environment: entanglement generation

The study of the environment that coupled to a quantum system does not only allow a better understanding of the decoherence mechanism discussed above. As a matter of fact, we can make use of the complete knowledge of the system-environment wavefunction to design meaningful and practical quantum operations. To illustrate this point, consider a simple three level system depicted in Fig. (1.4). It is coupled to the background of electromagnetic vacuum through the light-matter interaction. If we are not interested in the environment and simply ignore its information by tracing over the environmental degrees of freedom, an initially excited three level system simply relaxes to its ground state through spontaneous emission. This is just a simple decoherence process. On the other hand, however, provided with the knowledge of the total wavefunction of the system, the three level system can in principle decay to a superposition of two orthogonal spin ground

states $|+(-)\rangle$ by emitting a photon with different polarization $|H(V)\rangle$. This eventually leads to an maximally entangled Bell state between the qubit state and the emitted photon state, in the form of $(|+\rangle|H\rangle + |-\rangle|V\rangle)/2$. [10]

This allows a simple entanglement generation between a matter qubit and a single photon [10, 11]. Based on similar single photon ideas, it has been shown that one can perform quantum communication between qubit systems [12], generate entanglement between atomic ensembles [13], or between qubits at a distance [14], etc.

Yet, these quantum operation schemes are all based on the interaction bewtween a qubit and a single photon. The potential usefulness of the multiphoton environment has not been really made use of. In chapter 4, we will introduce a new protocol to generate quantum entanglement between distant qubits based on their couplings to the multiphoton environment. When the qubits are continuously driven at resonance, they emit fluorescence photons that carries information of the qubit state. We demonstrate how the qubit entanglement can be achieved by projection measurements of the fluorescence photons. Large improvements in entanglement efficiency and average entanglement rate are achieved, in comparison with the single photon protocol.

Bibliography

[1] R. P. Feynman, "Simulating physics with computers", Int. J. Theor. Phys. **21**, 467 (1982).

[2] P. W. Shor, "Algorithms for quantum computation: discrete logarithms and factoring", Proceedings of the 35th Annual Symposium on Foundations of Computer Science, 124 (1994).

[3] L. DiCarlo, J. M. Chow, J. M. Gambetta, L. S. Bishop, B. R. Johnson, D. I. Schuster, J. Majer, A. Blais, L. Frunzio, S. M. Girvin and R. J. Schoelkopf, "Demonstration of two-qubit algorithms with a superconducting quantum processor", **460**, 240 (2009).

[4] P. Maunz S. Olmschenk, D. Hayes, D. N. Matsukevich, L. M. Duan and C. Monroe, "Heralded Quantum Gate between Remote Quantum Memories", Phys. Rev. Lett. **102**, 250502 (2009).

[5] N. Lee, H. Benichi, Y. Takeno, S. Takeda, J. Webb, E. Huntington and A. Furusawa, "Teleportation of Nonclassical Wave Packets of Light", Science **332** 330 (2011).

[6] P. Aliferis, F. Brito, D. P. DiVincenzo, J. Preskill, M. Steffen and B. M. Terhal, "Fault-tolerant computing with biased-noise superconducting qubits: a case study", New J. Phys. **11**, 013061 (2009).

[7] R. P. Feynman and F. L. Vernon, Jr., "The Theory of a General Quantum System Interacting with a Linear Dissipative System", Annals of Physics **24**, 118 (1963).

[8] C. Gardiner and P. Zoller, *Quantum Noise: A Handbook of Markovian and Non-Markovian Quantum Stochastic Methods with Applications to Quantum Optics* (Springer, New York, 2000)

[9] H.-P. Breuer and F. Petruccione, *Theory of Open Quantum Systems* (Oxford Univ. Press, New York, 2002).

[10] S. E. Economou, R. B. Liu, L. J. Sham, and D. G. Steel, "Unified theory of consequences of spontaneous emission in a Λ system", Phys. Rev. B **71**, 195327 (2005).

[11] See for example, E. Togan, Y. Chu, A. S. Trifonov, L. Jiang, J. Maze, L. Childress, M. V. G. Dutt, A. S. Sørensen, P. R. Hemmer, A. S. Zibrov1 and M. D. Lukin, "Quantum entanglement between an optical photon and a solid state spin qubit", Nature **466**, 730 (2010).

[12] Wang Yao, Ren-Bao Liu and L J Sham, "Theory of control of the dynamics of the interface between stationary and flying qubits", J. Opt. B: Quantum Semiclass. Opt. **7**, S318 (2005).

[13] L.-M. Duan, M. D. Lukin, J. I. Cirac and P. Zoller, "Long distance quantum communication with atomic ensembles and linear optics", Nature **414**, 413 (2001).

[14] L.-M. Duan, M. J. Madsen, D. L. Moehring, P. Maunz, R. N. Kohn, Jr., and C. Monroe, "Probabilistic quantum gates between remote atoms through interference of optical frequency qubits", Phys. Rev. A. **73**, 062324 (2006).

Chapter 2

Precision of electromagnetic control of a quantum system in a non-Markovian environment

Coherent control of a quantum system is limited both by the decoherence due to environment and the quantum nature of the control agent. The high fidelity of control demanded by fault tolerant quantum computation and the intrinsic interest in nonclassical effects from the interplay between control and dissipation are motivations for a detailed study of the interaction dynamics between the quantum system and the macroscopic environment and control agent. In this chapter, we present a detailed time evolution study of a two-level system interacting with a laser pulse and the electromagnetic vacuum in the multimode Jaynes-Cummings model. A diagrammatic formalism allows easy identification of coherent dynamics and relaxation of the two-level system. We demonstrate a computational method of dynamics with precise error bounds for fast operations versus slow decoherence, spanning the Markovian and non-Markovian regimes. Comparison against an exact model solution of our results with existing approximations of the master equation shows the lack of accuracy in the latter.

2.1 Introduction

An open system, i.e., a small quantum object in the presence of a macroscopic environment, presents a fundamental problem in quantum mechanics and its applications. We wish to address here the problem of the environment with the dual function of decoherence and control of the quantum object. For practical purposes, both experiments on coherent processes and quantum technology require a small parameter t_0/T_2 in the time scale of the control duration t_0 being much smaller than the decoherence time T_2. A paradigmatic system for this problem is the interaction of a two-level system (TLS) with the quantized electromagnetic fields.[1] In terms of the TLS-photon interaction strength g in units of frequency, the controlled TLS process (the Rabi rotation) is a strong coupling process with $g|\alpha|t_0 \sim O(1)$ using a coherent photon state $|\alpha\rangle$ with a large mean number $|\alpha|^2$ of photons while the long decoherence time is a weak coupling process $t_0/T_2 \ll 1$ within the control time. In particular, the high fidelity of the operation to an error threshold between 10^{-3} and 10^{-4} in fidelity demanded by fault tolerant quantum computation[2, 3] sets the bar for high accuracy in the theory of the open system. While the TLS open system problem has been much studied, we posit that the specific additive problem of the control and decoherence processes remains.

The decoherence problem of a TLS in a spin bath and its suppression under a classical control have been extensively studied,[4, 5] but the noise due to a quantized optical control was not taken into account. Barnes and Warren demonstrated the decoherence induced by the back action from the TLS to the electromagnetic control.[6] For a Markovian system, this problem can be solved using the optical Bloch equation[7]. However, in many non-Markovian systems with a structured environment, say nanocavities[8] and photonic band gap materials[9], the optical Bloch analysis no longer applies. Because of the large Hilbert space of the multimode TLS-field Hamiltonian, an exact diagonalization of the problem is impractical.[10] Therefore, a quantum theory suitable for a non-Markovian open system with high accuracy set for our problem is needed.

In this chapter, we develop a formalism to solve the multimode Jaynes-Cummings (JC) model under a coherent light pulse with arbitrary pulse shape in

the limit $t_0 \ll T_2$, relevant to the problem posed. The exact non-unitary evolution of the TLS is expressed in terms a time evolution forward and a reverse evolution backward of emitted and absorbed photons conditioned on the TLS down and up transitions. The photon dynamics are evaluated by the field theoretic perturbation series. The diagrammatic structure allows an explicit identification of the photons' role in coherent dynamics and dissipation process of the TLS. All perturbation terms in a coherent dynamics segment are summed and the dissipative processes are expanded in powers of a small parameter $(t_0/T_2)^\gamma$ where γ depends on the photon correlation time τ_c and ranges between 1 (the Markovian limit) and 2 (the non-Markovian limit). The process gives a practical numerical computation procedure for a given error limit in powers of the small parameter. We illustrate the computation for a short-time quantum operation of the TLS by including all the relevant quantum processes within the first order error bound. We identify the precise origins of the interference effects between the control and the dissipation in the evolution processes.

The master equation (ME) approach of treatment of the open quantum system has been enormously important for quantum optics [11] and for quantum information.[12] We have made a comparison of our theory with several prominent approximations extant in the ME approach[13] for a model problem involving the interference effect between control and decay which has an exact solution and a semiclassical one. The comparison results show that in the non-Markovian regime, the driving forces for the coherent control and the dissipation are not additive and that the ME approximations are closer to the semiclassical results than the quantum results, not meeting the stringent accuracy requirement. Perhaps, the comparison results would stimulate effort to refine the ME approximations.

The outline of the rest of the chapter is as follows. In Section 2.2, we develop a field-theoretic solution for the JC model in the presence of the multi-mode photonic field, elucidating the coherent and dissipative components from the diagrammatic structure. In Sec. 2.3, a detailed analysis of the effect of vacuum decoherence on the control precision of the TLS is given in the non-Markovian regime. Sec 3.3 compares the diagrammatic solution with the ME approximations.

Sec. 3.5 summarizes and the appendices add some technical details.

2.2 TLS-photons interaction dynamics

By the field theoretic techniques, we express the evolution operator of the whole system (the TLS and the photons) as an infinite perturbation series in terms of the spin and photon operators. Then, we evaluate the matrix elements of the spin exactly, resulting in a diagrammatic series of the photon operators only. By the Wick's theorem on the photon operators, we build a perturbative solution to the non-equilibrium problem of the dynamics of the laser photons and the TLS in the bath of the electromagnetic vacuum. We find a controlling small parameter, $(t_0/T_1)^\gamma$, defined in the Introduction and detailed below, for the perturbation series. The approach of removing the spin operators first stands in contrast to the standard ME approach[13] which traces out the photonic environment first and then solves the equation of motion of the TLS, and which lacks error bounds for most of its approximations.

2.2.1 TLS transformation by coherent photon state

We start with the canonical multimode JC Hamiltonian:[1, 14]

$$\begin{aligned} H &= H_0 + V, \qquad (2.1)\\ \text{where} \quad H_0 &= \frac{1}{2}\omega_0\sigma_z + \sum_k \omega_k a_k^\dagger a_k,\\ V &= \sum_k g_k\Big(\sigma_+ a_k + \sigma_- a_k^\dagger\Big). \qquad (2.2) \end{aligned}$$

H_0 contains the bare Hamiltonian of the TLS of energy splitting ω_0 with the Pauli operator σ_z and the photons of energy ω_k with creation operator $a_k^\dagger$. V is the TLS-photon interaction with the coupling constant g_k, presented in the rotating wave approximation (RWA) which is justified in Appendix 2.7.1. While the single-mode JC may be used to treat the laser pulse by making the coupling time-dependent $g(t)$, the multimode extension [7] is more suited for our purpose of investigating the joint quantum effects of the light control of TLS and the dissipation.

The composite system of the TLS and photons is given by a product initial wavefunction, $|\Psi(0)\rangle = [\sum_s c_s|s\rangle]\,|\boldsymbol{\alpha}\rangle$, where $s = \pm$ denotes the two states of the TLS and $\boldsymbol{\alpha} = (\alpha_{k_1}, \alpha_{k_2}, \ldots)$ denotes the multimode coherent state. The reduced density matrix $P_{s_f,s'_f}(t)$ is expressed in terms of the transformation matrix conditioned on the initial photon state:

$$
\begin{aligned}
P_{s_f,s'_f}(t) &= \sum_{s,s'} c_s c^*_{s'} p_{s_f,s'_f;s,s'}(t,\boldsymbol{\alpha}) && (2.3)\\
p_{s_f,s'_f;s,s'}(t,\boldsymbol{\alpha}) &= \langle\boldsymbol{\alpha}|\langle s'|U^\dagger(t)|s'_f\rangle\langle s_f|U(t)|s\rangle|\boldsymbol{\alpha}\rangle \\
&\quad \times\ e^{i(s'_f 1 - s_f 1)\omega_0 t/2}. && (2.4)
\end{aligned}
$$

In the interaction picture, the time evolution operator and the interaction are:

$$
\begin{aligned}
U(t) &= T\exp\Big[-i\int_0^t dt' V(t')\Big], \\
V(t_l) &= \sigma_+ A_l + \sigma_- A_l^\dagger, && (2.5)\\
\text{where}\quad A_l &= \sum_k g_k a_k e^{i\Delta_k t_l}, \\
A_l^\dagger &= \sum_k g_k a_k^\dagger e^{-i\Delta_k t_l}, && (2.6)
\end{aligned}
$$

and $\Delta_k = \omega_0 - \omega_k$ is the detuning of the k mode. This form of transformation of the reduced density matrix visibly retains the quantum nature of the evolution of the composite system and is easily reduced to the problem of the expectation value of the electromagnetic field operators for the initial photon state. The initial product state may be generalized to any composite state $|\Psi(0)\rangle = \sum_s \int \mathbf{D}\boldsymbol{\alpha} c_{s,\boldsymbol{\alpha}}\,|s\rangle\,|\boldsymbol{\alpha}\rangle$, where $\int \mathbf{D}\boldsymbol{\alpha} = \int \frac{d^2\alpha_{k_1}}{\pi}\frac{d^2\alpha_{k_2}}{\pi}\ldots$

In the perturbation series of the evolution operator, the TLS state is flipped up or down by a series of interaction, leaving only the corresponding photon oper-

ators,

$$\langle \pm|U(t)|\pm\rangle = \sum_{n=0}^{\infty}(-i)^{2n}\int_0^t D^{2n}t\ X_{2n}^{\pm}, \tag{2.7}$$

$$\langle \mp|U(t)|\pm\rangle = \sum_{n=0}^{\infty}(-i)^{2n+1}\int_0^t D^{2n+1}t\ X_{2n+1}^{\pm}, \tag{2.8}$$

$$\begin{aligned}
\text{where}\quad \int_0^t D^n t &= \int_0^t dt_n ... \int_0^{t_3} dt_2 \int_0^{t_2} dt_1, \\
X_{2n}^{+} &= A_{2n}A_{2n-1}^{\dagger}\ ...\ A_2 A_1^{\dagger}, \\
X_{2n+1}^{+} &= A_{2n+1}^{\dagger}X_{2n}^{+}, \\
X_{2n}^{-} &= A_{2n}^{\dagger}A_{2n-1}\ ...\ A_2^{\dagger}A_1, \\
X_{2n+1}^{-} &= A_{2n+1}X_{2n}^{-}.
\end{aligned} \tag{2.9}$$

2.2.2 TLS evolution in terms of photon processes

The task is reduced to evaluate the transformation matrix in Eq. (3.5) in terms of the series expansion of the unitary operator and its inverse in Eq. (2.7) or (2.8) that consist of photonic components in Eqs. (2.9). The formulation is exact so far. The evaluation of the series is simplified by the Wick's theorem [15] (see Appendix 2.7.2). Each series term in Eq. (2.7) is of the form $X_m^{\pm\dagger}X_{m'}^{\pm}$ from Eqs. (2.9), a product of several photon operators A_i and$A_j^{\dagger}$, which the Wick's theorem resolves into a sum of terms composed of a normal product and a number of pairs of contractions. The matrix element of each normal product between two coherent states is simply products of scalars from the substitution of $a_k \to \alpha_k$ acting on the coherent ket vector and $a_k^{\dagger} \to \alpha_k^*$ acting on the bra vector. The contractions from Eq. (2.20) are

$$\langle A_i^{\dagger}A_j\rangle = 0, \tag{2.10}$$

$$\langle A_i A_j^{\dagger}\rangle = K(t_i - t_j) = \sum_k |g_k|^2 e^{i\Delta_k(t_i - t_j)}. \tag{2.11}$$

Fig. 2.1 illustrates the diagrammatic representation of each term in the series expansion of the transformation matrix and some partial summations of subseries. Fig. 2.1(a) shows a typical term. The rules are: (i) the initial and final

TLS states represented at times 0 and t, (ii) the interactions with the TLS denoted by dots in the counterclockwise loop for the time-ordered photon operators from time $0 \to t$ and then in anti-time order back $t \to 0$, (iii) the appropriate TLS states between dots labeled as $\pm$ and (iv) all possible contractions (dashed lines) either on the same time line or between the opposite time lines. Fig. 2.1(b) shows the only two possible types of contractions because of Eqs. (2.10,2.11). If the two ends of a solid line segment have the same (opposite) TLS states, the segment is dressed by an even (odd) number of photons whose series sum is depicted by a double (triple) line, see Fig. 2.1(c). Fig. 2.1(d) provides an example of the transformation matrix $p_{++,++}$ with a single contraction and dressed states. We stress that these diagrams are first order in contraction, but infinite order in the coherent interaction.

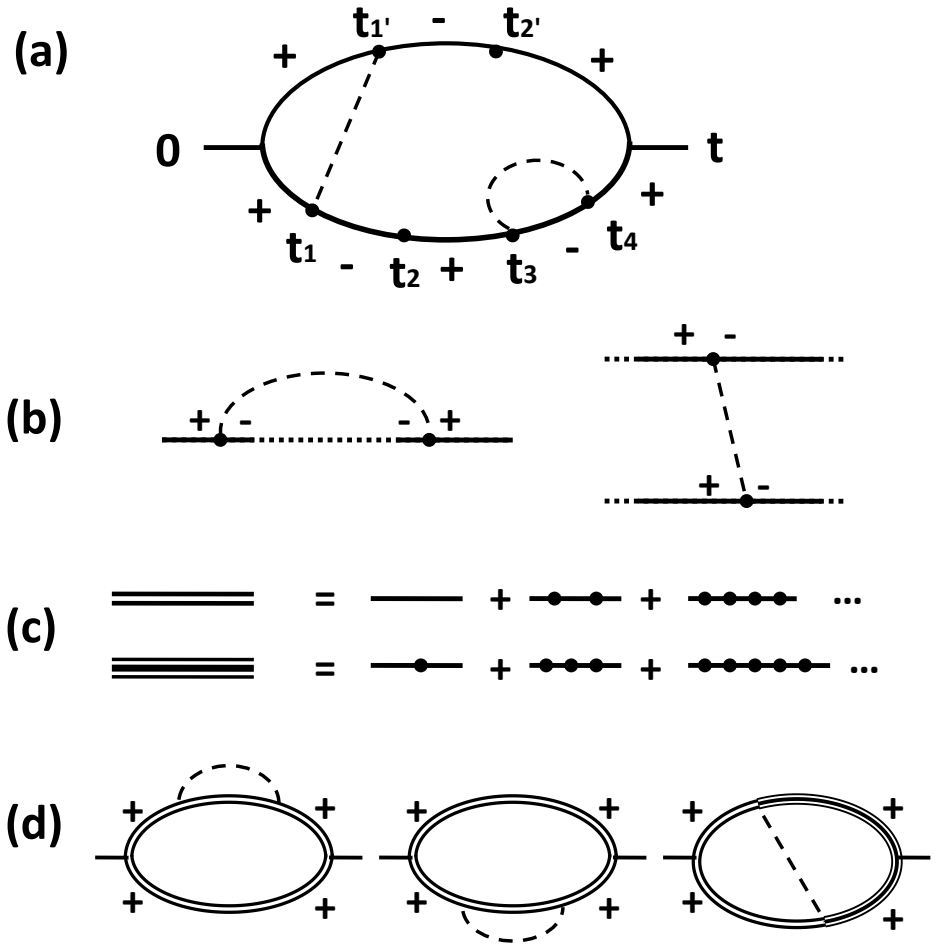

Figure 2.1: Diagrammatic representations of perturbation terms of the transformation matrix $p_{s_f,s'_f;s,s'}(t,\{\alpha\})$. (a) An example of six photon operators with two contractions. The two short lines labeled $0, t$ are the time limits of the integrals. Each dot labeled with a time variable t_n represents one photon operator, the lower solid arc being time ordered and the upper arc anti-time-ordered. A dashed line stands for one contraction between two photonic operators. The uncontracted dots form a normal product of the photon operators for the matrix element of the coherent states. The $\pm$ sign denotes the state of the TLS at different times. (b) The only possible contractions drawn between photons on the same or opposite time lines. (c) The dressed line by a sum of all even or all odd numbers of photons interacting with TLS without contraction. (d) Three diagrams that contains only a single contraction for the transformation matrix $p_{++;++}$. They are the leading contributions to the control noise.

2.2.3 The key results

The quantum treatment of the time evolution of the TLS in terms of a series of photon contractions yields a number of notable results. The series expansion in the TLS-photon interaction permits identification of the physical processes. Well-known are the all-dots terms uninterrupted by dotted lines, as in the first term of Eq. (2.19) whose sum yields the Rabi rotation and the complete contraction pairs in the last term of the same equation whose sum yields the relaxation due to the electromagnetic vacuum (see Appendix 2.7.3). In the mixed terms, the dots between the ends of contractions may still be summed as coherent dynamics of the TLS. The summation is necessary because along the dressed line, each photon gives a term of the order $g|\alpha|t_0$ for a pulse of duration t_0. These series expressions can be summed exactly and are given in Appendix 2.7.3. The coexistence of the coherent dynamics and relaxation yields an effect which is extra to the sum of the two processes, as will be shown next. This is also clear in the nature of the contraction between the evolution and its inverse shown in Fig. 2.1(a) and (d). Note how, without the manual separation of the photon Hamiltonian into a control part and a bath part, the method produces the dissipation and the Rabi rotation. More importantly, it contains quite explicitly the interference effects between the two processes.

A useful result for our stated purpose of studying the fidelity of the control process to high accuracy is the finding of a small parameter for the expansion. After the construction of the dressed lines of the coherent processes, the expansion of the contraction functions is a perturbation series in powers of $(t_0/T_1)^\gamma$ in terms of the operation time t_0 and the decay time T_1 (see Appendix 2.7.3 for the decoherence time $T_2 = 2^{1/\gamma}T_1$). The decay in each contraction line is $\sim \int\int dt_i dt_j K(t_i - t_j) \sim O[(t_0/T_1)^\gamma]$, where the parameter γ between $(1, 2)$ depends on the shape of the photon DOS. Therefore, this method provides an excellent evaluation of the control noise in the regime $t_0 \ll T_1$, while the area of the pulse $\sim g|\alpha|t_0 \sim O(1)$. The one-contraction terms in Fig. 2.1(d) together give the consistent result to the first order contribution of the control noise which will be evaluated next. The consistency of the three diagrams comes from the differentiation of a self-energy diagram with

one contraction resulting in three terms, as in the Ward identity in field theory. [16]

2.3 Relaxation and control fidelity

The quantum effects between the coherent control and the vacuum decoherence depend crucially on the contraction, which, Eq. (2.11) shows, depends on the materials properties of the TLS and the photon confinement in the form of the DOS of the photonic field weighed by the interaction mode dependence. To show explicitly the dependence of the control dynamics on the weighted DOS, it is convenient to model it as a Gaussian:

$$\rho(\omega) = \sum_k g_k^2 \delta(\omega - \omega_k) = \frac{g^2 \tau_c}{2\sqrt{\pi}} e^{-\tau_c^2 (\omega - \omega_0)^2/4}, \tag{2.12}$$

where g is the average coupling strength and τ_c describes the correlation time of multimode light in the presence of a TLS. The qualitative results, such as the concept of the exponent γ in decay, are unchanged for a general DOS that includes a correct behavior for $\omega \to 0^+$. When $\tau_c \to 0$, the broadband DOS yields $T_1 = 1/\sqrt{\pi} g^2 \tau_c$; while as $\tau_c \to \infty$, the single mode scenario pertains. Under this Gaussian DOS, Eq. (3.8) shows that the contraction function is also a Gaussian, i.e., $K(t) = g^2 e^{-t^2/\tau_c^2}$.

For a broadband DOS, e.g., in free space, the system is Markovian and the result is equivalent to that from solving the optical Bloch equations.[7] For an extremely narrow DOS, single-mode cavity quantum electrodynamics dominates. In this section, we use a Gaussian DOS whose variable width causes the decay of the upper state of the TLS to have a dependence of $\ln P_{++}(t) \propto -(t/T_1)^\gamma$ characterized by the exponent γ and use the change of the system from the exponential decay ($\gamma = 1$) in the broad DOS limit to a Gaussian decay ($\gamma = 2$) in the narrow DOS region to show the emergence of the quantum effects of interference between the laser control and the vacuum decoherence. The interference actually has a beneficial effect on the fidelity of the quantum operation on the TLS.

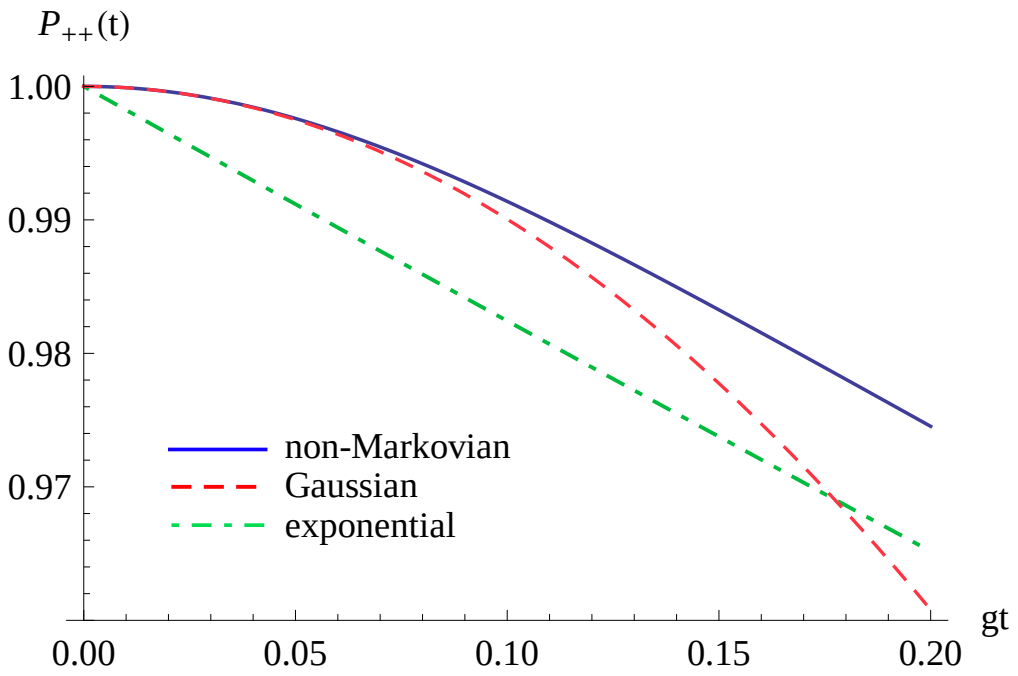

Figure 2.2: Relaxation of an initially excited TLS state in vacuum using a Gaussian photon DOS with $g\tau_c = 0.1$. The decoherence of the TLS (solid curve) is different from the purely Gaussian (dashed) or Markovian (dash-dotted) decay.

An example of a relevant physical system is a multimode finite Q cavity system with bandwidth $\sim 1/t_0$. For a photonic crystal nanocavity[8] with $Q \sim 10^4$–10^5 and $\omega_0 \sim 10^{15}$ Hz, the estimated value of τ_c is ~ 100 ps and non-Markovian features could be observable for $t_0 \sim \tau_c$. Then, the small parameter condition for a fidelity of 0.9999 could be relaxed from $t_0/T_1 \sim 10^{-4}$ to 10^{-2}.

2.3.1 Non-markovian relaxation for a Gaussian DOS

The short time decoherence behavior of the non-Markovian multimode JC system in vacuum is given by diagrams with only one contraction (see Fig. 2.7(b)). For an initially excited TLS, we have

$$\ln[P_{++}(t)] \approx -2\int_0^t dt_1 \int_0^{t_1} dt_2 K(t_1 - t_2). \tag{2.13}$$

An illustration using $g\tau_c = 0.1$ is presented in Fig. 2.2. The result reveals that for a finite value of τ_c, the system evolves from a non-Markovian Gaussian dependence

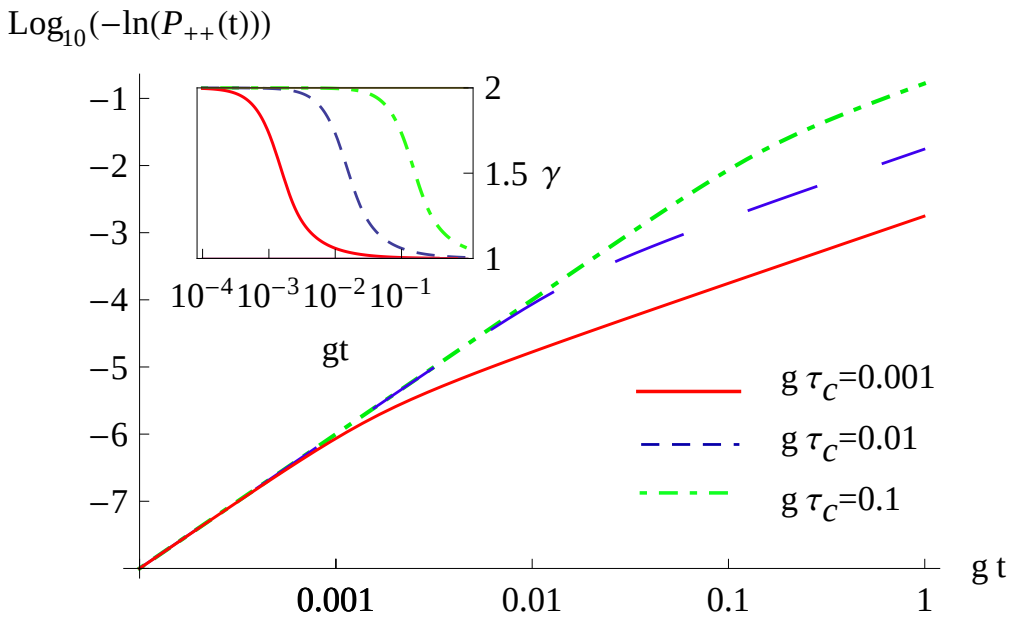

Figure 2.3: Plots of $\log_{10}\left[-\ln P_{++}(t)\right]$ in short time for different values of correlation τ_c. Crossover between Markovian and non-Markovian relaxation occurs at $t \sim \tau_c$. The inset shows the decay exponent, γ.

(well-known in the onset of the collapse and revival phenomena,[14, 17, 18, 19]), $P_{++}(t) \approx e^{-(gt)^2}$, to the Markovian exponential decay, $P_{++}(t) \approx e^{-t/T_1}$. The crossover takes place at $t \sim \tau_c$. For short time, the contraction function is almost flat and the decay resembles the single mode case. As time increases and exceeds τ_c, the Gaussian contraction function approaches the broadband Markovian limit. Note that both the Markovian and single mode approximations overestimate the decoherence of the TLS.

Fig. 2.3 depicts the evolution of $P_{++}(t)$ in the log scale for different $g\tau_c$. It shows the same crossover from the non-Markovian to Markovian relaxation when time is comparable to the correlation time. The decay exponent γ, defined by $P_{++}(t) \approx e^{-(t/T_1)^\gamma}$ can vary from 2 to 1 as time increases. Because of this non-Markovian dynamics, the fidelity of the TLS under a coherent control also shares the same feature. We will investigate this more quantitatively in the next subsection.

2.3.2 Control fidelity analysis

The control noise problem is solved by the diagrammatic method in Sec. 2.2 with TLS initially in the excited state and under a coherent 2π pulse with truncated Gaussian shape defined by $\Omega(t) = \Omega\ e^{-(t-\frac{t_0}{2})^2/\sigma^2}$ for $0 < t < t_0$ and zero otherwise. The coherent state amplitudes α_k is related to $\Omega(t)$ by Eq. (3.4). We take $\sigma = t_0/4$ and use the Gaussian photon DOS given by Eq. (2.12).

We evaluate the single contraction diagrams in Fig. 2.1(d) for decoherence of $\sim O[(t/T_1)^\gamma]$. The fidelity is computed by $F(t = t_0) = Tr\,[P_{ideal}P(t = t_0)]$, where P_{ideal} is the ideal reduced density matrix. The error, $1 - F(t = t_0)$ is plotted as a function of control duration gt_0 in Fig. 2.4 and is compared with the Markovian (i.e. broadband) approximation. The third diagram in Fig. 2.1(d) gives a contribution from the contraction between two time lines which tends to be opposite in sign to the dissipation effect of the two graphs with contractions within the the same line. This is evidence of quantum interference between control and dissipation. Owing to the non-Markovian relaxation, the error of the operation goes quadratically with t_0 for small t_0 and then becomes linear in t_0, which is different from the linear t_0 dependence in the Markovian limit. The crossover occurs at $t_0 \sim \tau_c$ for the same physical reason in the vacuum relaxation process. The fidelity is in the form, $F = 1 - c(t_0/T_1)^\gamma$, where $1 \leq \gamma \leq 2$ and c is a constant.

The relaxation at $t > t_0$ after the pulse finishes is not as simple as the Markovian limit, and is given by

$$P_{\sigma\sigma'}(t > t_0) = P_{\sigma\sigma'}(t = t_0) - f_{\sigma\sigma'}[\mathcal{A}(t)] \times [(t - t_0)/T_1]^\gamma\,. \tag{2.14}$$

The renormalization factor $f_{\sigma\sigma'}[\mathcal{A}(t)]$ is a functional of $\mathcal{A}(t)$, depending on the shape of the pulse. This reflects the history-dependent dynamics of the TLS when we consider a Gaussian photon DOS. Such a feature stands in contrast with the Markovian case, where the function $f_{\sigma\sigma'}[\mathcal{A}(t = t_0)]$ only depends on the total area of the pulse.

The discussion above is based on a pure starting state. Consider the extension to a mixed starting state. Let the prepared pure state at $t = 0$ relax to the mixed state at time $t_i > 0$ when a control operation starts. Then, the TLS is

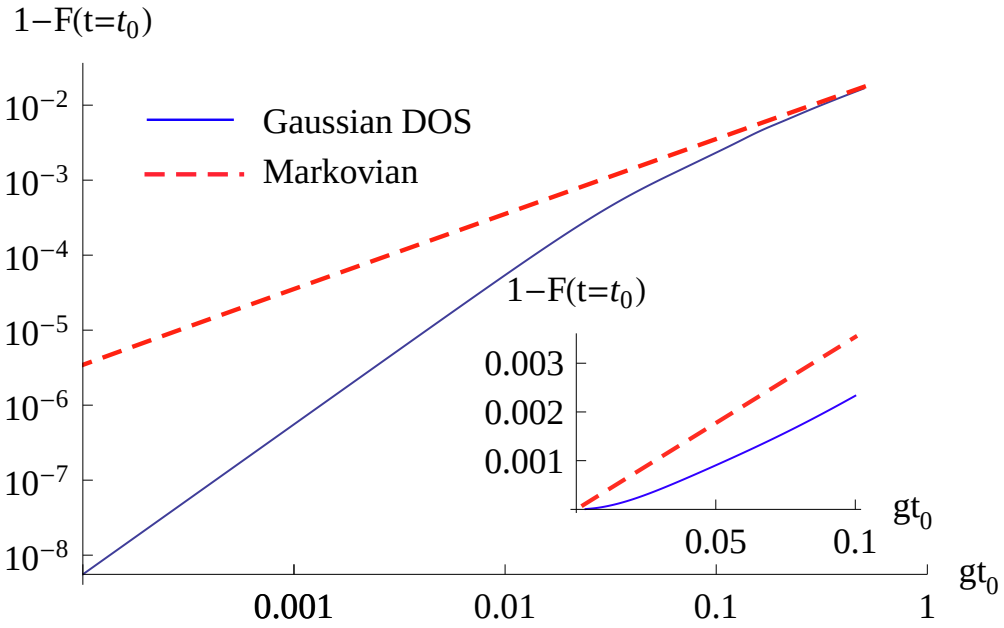

Figure 2.4: A plot of error, $1 - F(t = t_0)$ for a TLS driven by a nominal 2π Gaussian pulse using a Gaussian DOS with $g\tau_c = 0.03$ (solid blue) and a constant DOS (dashed red). For the Gaussian DOS, the t_0 dependence of error changes from quadratic to linear when $t_0 \sim \tau_c$, whereas the error depends linearly on t_0 in the Markovian regime.

driven by the control pulse and influenced by the vacuum decoherence. The theory is the same except the laser pulse is shifted in time to $\Omega(t) \neq 0$ in $t_i \leq t \leq t_f$. The fidelity of an example is studied, using a 2π pulse, which is Gaussian cut off at both ends of the same time interval σ from the center as before. The results are given in Fig. 2.5 for the relative error defined as the proportionate change of state fidelity between the start and the finish of the pulse, $R_F = 1 - [F(t_f)/F(t_i)]$ of the operation as a function of the initial time of the pulse. For a small and fixed duration $t_0 = t_f - t_i$, we observe that the relative error increases linearly with t_i and then saturates to a constant after $t_i \sim \tau_c$. This can be roughly understood by employing the decoherence crossover picture discussed in subsection 2.3.1. When the operation is performed inside the non-Markovian region, $F \sim e^{-(gt_i)^2}$ and $R_F \sim 2g^2 t_0 t_i$; whereas in the Markovian limit, $F \sim e^{-t_i/T_1}$ and $R_F \sim t_0/T_1$.

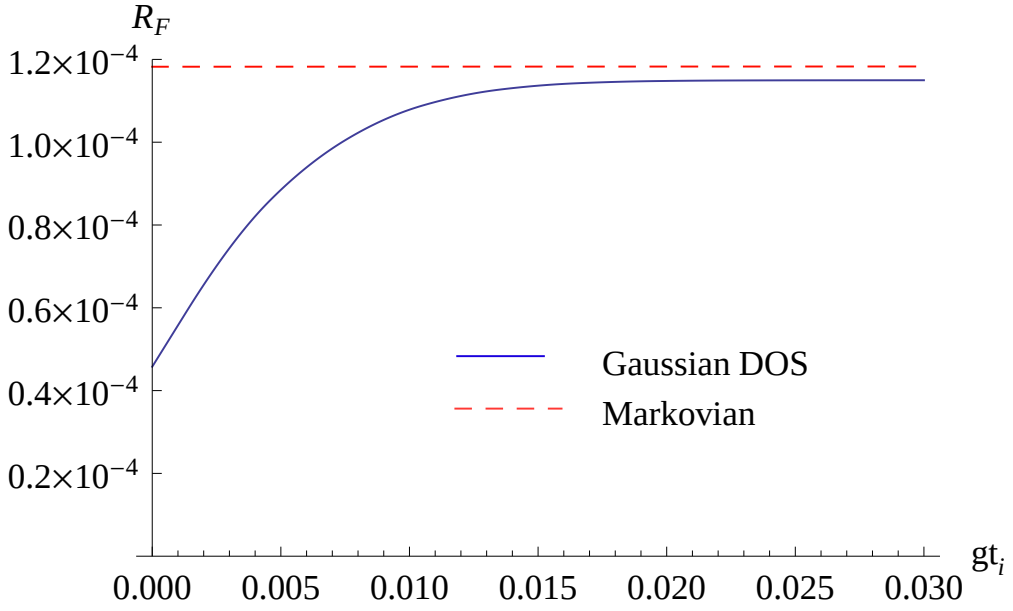

Figure 2.5: Relative error, $R_F = 1 - F(t_f)/F(t_i)$ as a function of t_i of a TLS under a 2π Gaussian pulse for fixed $gt_0 = g(t_f - t_i) = 0.01$ and $g\tau_c = 0.01$. For a Gaussian DOS, a change of dependence on t_i occurs when the system evolves from the non-Markovian to Markovian regime.

2.4 Error checks

We check our method against the exact solution, [14] of the driven single-mode JC model for the non-Markovian effects involving control and decay of the TLS and compare with approximations in the master equation approach. It is a limit of the multimode problem for $g\tau_c = \infty$ and $\gamma = 2$. We choose four commonly used ME approximations, (i) the Born series, (ii) the Nakajima-Zwanzig (NZ) projection method, (iii) time-convolutionless (TCL) projection[20, 13], and (iv) the additive assumption.[21] Unlike our error bound, these theories contain none. Their results are compared with the exact, the diagrammatic and the classical Rabi solutions. For details of how the first three methods are used in the calculations, see Appendix 2.7.4. The additive ME, assumes that the driving terms of the equation of motion by control and by dissipation simply add:

$$\frac{d}{dt}\rho_s(t) = -i[H_{cl}(t), \rho_s(t)] + \hat{K}\rho_s(t), \tag{2.15}$$

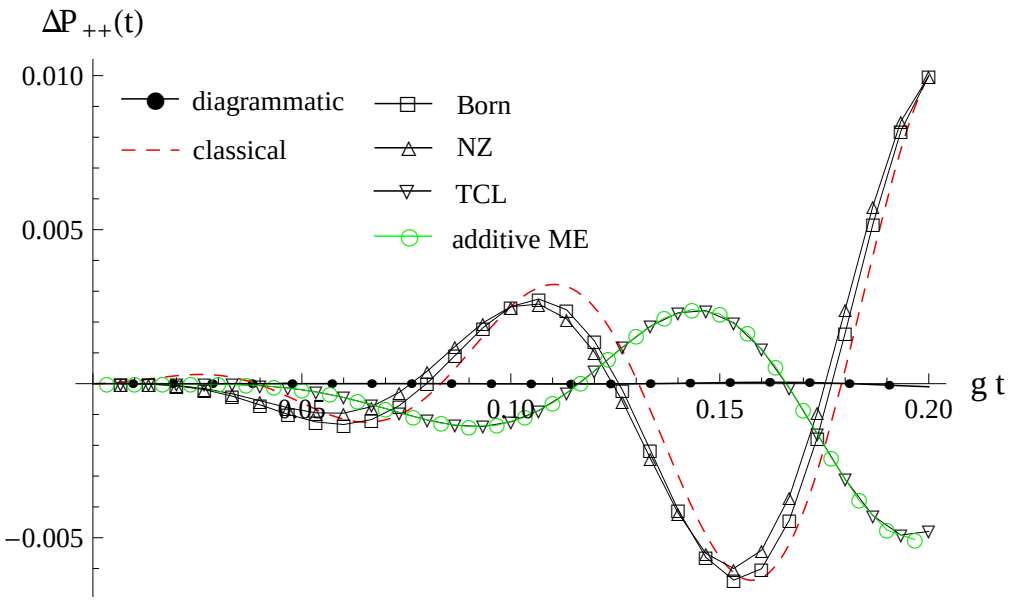

Figure 2.6: $\Delta P_{++}(t)$, the deviation of $P_{++}(t)$ from the exact solution of a driven single mode JC system using different methods. $\bar{n} = 100\pi^2$, corresponding to a 4π rotation at $gt = 0.2$. The errors of the ME approximations are as much as that of the classical solution.

where $\rho_s(t)$ is the reduced density matrix of the TLS, $H_{cl}(t)$ the classical control Hamiltonian, and $\hat{K}$ an appropriate super-operator on $\rho_s(t)$ for the population decay and decoherence effect in the absence of a control (see Appendix 2.7.4).

The TLS is initially in the excited state and driven by a single mode coherent state at resonance with the TLS. The average number of photons, $\bar{n} = 100\ \pi^2$, is chosen so that, at $gt = 0.2$, the area of the classical pulse is 4π. Fig. 2.6 plots the deviations of the upper state population from the exact solution, $\Delta P_{++}(t) = P_{++}(t) - P_{++}^{\text{exact}}(t)$, for the six methods above. The diagrammatic method is indistinguishable from the exact solution in the small parameter region of $gt \leq 0.2$ with a theoretical error bound $\sim O[(gt)^4]$ and the actual computed results within an error of 10^{-4}. This error can be further improved to $O[(gt)^{2(n+1)}]$ by including higher order diagrams with n contractions. The Born approximation and the low order NZ give results close to the classical treatment of the electromagnetic fields can be interpreted as a lack of quantum content. The agreement between the low order TCL and the additive approximation might be an indication of the addi-

tive nature of TCL. All four ME approximations fail to reproduce the quantum interference effects between control and dissipation which are in the field theoretic treatment. Note that the problems of the NZ and TCL methods are not due to the second order approximation we used because their errors are also of the same order. The failure of the ME methods to account for the high accuracy of control fidelity required by quantum information processing is illustrated by this comparative study.

2.5 Summary

We have developed a rigorous solution of the multimode Jaynes-Cummings model for a two-level system under the control of a coherent electromagnetic pulse. It treats the control process exactly within a rigorous error bound for the controlled dynamics of the entire system of the small quantum object and the photons to any order in the small parameter in operation time versus the decoherence time, $(t_0/T_2)^\gamma$ where γ varies from 1 to 2 as the density of states of the photons varies from being flat as in free space to a sharp peak as in high Q cavity. Our theory is quantum in the sense of no stochastic assumption and treats the entire quantum system correctly within any given error bound. A diagrammatic representation provides a simple picture of different physical processes, including the familiar limiting cases of coherent Rabi oscillation and vacuum decoherence. It pinpoints the control-dissipation interference as the quantum effects found by works which precede ours [22]. The effects are relevant to basic quantum phenomena and to technological applications.

This work shows that vacuum relaxation is not the only physical process that results in quantum noise in non-Markovian systems. Fundamental quantum noise due to interference between the control field and relaxation exists and it leads to a decoherence comparable to the vacuum fluctuations. Moreover, our method is not restricted to the Markovian limit and is valid for an arbitrary DOS. Thus, it necessarily goes beyond the optical Bloch analysis.

The time evolution study shows that the relaxation of the TLS can vary

from a Gaussian decay to an exponential one, depending on the ratio of time to the correlation time that characterizes the photon DOS. In consequence, the fidelity of a general single qubit operation on a pure state can be cast in the form $F = 1 - c(t_0/T_2)^\gamma$ for a constant c. The Markovian approximation ($\gamma = 1$) overestimates the decoherence of the TLS. The Gaussian decoherence ($\gamma = 2$) provides a lower bound for the quantum error of a light controlled TLS.

The field theoretic technique provides a completely quantum mechanical description of a small quantum system interacting with the photonic environment. The control noise issue, being important in quantum computing, serves as an concrete example to demonstrate its capability. This approach may also be applied to other systems under nonclassical photon states. Besides the quantum object, the field theoretic technique also permits a calculation of the physical quantities of the environment, e.g. the quantum feedback on the electric field, photon correlation functions, correlation between the TLS and the photons, etc.

Comparative studies with the existing master equation approximations show their general lack of the quantum effects due to the control-dissipation interplay, which is not restricted to the single-mode model tested. We hope that the results of our rather cursory study of these approximations would stimulate more developments in rigorously bounded approximations for the master equation and further understanding of quantum effects by the contrast and complementarity between the master equation and the field-theoretic approaches.

Our current theory only considers a coherent state with a constant phase. In future work, this can be generalized to describe an ensemble of coherent states with a mixture of phases in order to evaluate the phase error as an extension of previous single mode study.[22]

2.6 Acknowledgments

This research was supported by the U.S. Army Research Office MURI award W911NF0910406. We would like to thank Paul R. Berman and Renbao Liu for helpful discussions. C. K. Chan thanks Wen Yang for a useful comment.

The text in chapter 2, in part, is a reprint of the material as it appears in Ching-Kit Chan and L. J. Sham, "Precision of electromagnetic control of a quantum system", Physical Review A **84**, 032116 (2011). The dissertation author was the first author of the paper and the co-author in this publication directed, supervised, and co-worked on the research which forms the basis of this chapter.

2.7 Appendix

2.7.1 Rotating wave approximation

To prove its validity for the control noise problem, we start with the Hamiltonian $H = H_0 + V$ in Eq. (2.1) with the full interaction term, $V = \sum_k g_k(a_k^\dagger + a_k)\sigma_x$. To this, we apply a unitary transformation e^S, where, [23]

$$S = \sum_k \frac{g_k}{\omega_k + \omega_0}(a_k^\dagger + a_k)\sigma_x. \tag{2.16}$$

For $g|\alpha|/\omega_0 \ll 1$, we expand the transformed Hamiltonian $\tilde{H} = e^S H e^{-S}$ up to second order in g_k as:

$$\begin{aligned} H &= H_0 + V_{\mathrm{RWA}}(\{g_k'\}) + V', & (2.17)\\ \text{where}\quad V' &= \frac{1}{4\omega_0}\sigma_z\Big[\sum_k g_k'(a_k^\dagger - a_k)\Big]^2. & (2.18) \end{aligned}$$

$V_{\mathrm{RWA}}(\{g_k'\})$ is the TLS-field coupling in RWA with g_k replaced by $g_k' = 2g_k\omega_0/(\omega_0 + \omega_k)$. Therefore, the counter-rotating terms leads to an effective perturbation V' as a correction to the RWA. It is an order $O(g\alpha/\omega_0)$ smaller than V_{RWA}. Hence, in the regime where $1/\omega_0 \ll 1/g|\alpha| \sim t \ll T_1$, the effect of the counter-rotating terms is negligible compared with decoherence.

2.7.2 Application of the Wick's theorem

The evaluation of the general perturbation term is simplified by the Wick's theorem, a general bosonic operator defined by $W = \prod_i O_i$, where $O_i = \sum_k (u_{ki}b_k +$

$v_{ki}b_k^\dagger$) is a linear combination of bosonic operators b_k and $b_k^\dagger$, and can be rearranged as: [15]

$$\begin{aligned} W = :W: &+ \sum_{(i_1,j_1)} :W_{i_1,j_1}: \langle O_{i_1} O_{j_1} \rangle \\ &+ \sum_{(i_1,j_1)\neq(i_2,j_2)} :W_{i_1,j_1,i_2,j_2}: \langle O_{i_1} O_{j_1} \rangle \langle O_{i_2} O_{j_2} \rangle \\ &+ \dots \\ &+ \sum_{(i_1,j_1)\dots(i_n,j_n)} \langle O_{i_1} O_{j_1} \rangle \dots \langle O_{i_n} O_{j_n} \rangle , \end{aligned} \tag{2.19}$$

where $:W:$ is the normal ordered form of W, defined by all the creation operators to the left of the annihilation operators; $:W_{j,k,l,\dots}:$ is the normal ordered form of $\prod_{i\neq j,k,l,\dots} O_i$ in which the operators O_j etc. are left out; and the contraction between O_i and O_j is defined only for $i < j$ by a scalar,

$$\langle O_i O_j \rangle = O_i O_j - :O_i O_j:, \tag{2.20}$$

Note that the suffix in the O operator denotes its order in the W expression, rather than the time index in the photon operator A_l.

2.7.3 Evaluation of control and dissipation

This supplements Sec. 2.3 with an analysis of the mathematical structure of the diagrammatic series, two examples of exactly soluble situations, and more details of the evaluation of formulas.

The contraction formula

Central to the vacuum decoherence is the contraction function from Eq. (2.11) given by,

$$\langle A(t) A(t')^\dagger \rangle \equiv K(t-t') = \int d\omega \rho(\omega) e^{i(\omega_0-\omega)(t-t')}, \tag{2.21}$$

where t and t' can be on the same or opposite time lines.

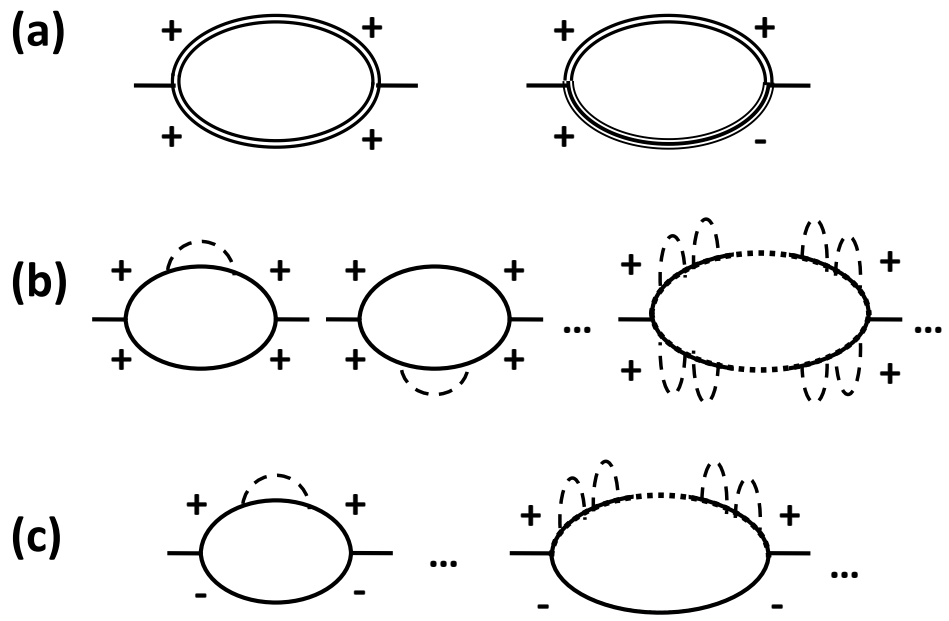

Figure 2.7: (a) gives the diagrams for the classical Rabi solutions for $p_{++,++}(t)$ and $p_{-+,++}(t)$. (b) and (c) provide all the diagrams in the absence of control for $p_{++,++}(t)$ and $p_{-+,-+}(t)$ respectively. In the Markovian limit, the two ends of a dashed line are squeezed to the same point. (b) consists of two lowest order diagrams while there is only one in (c), implying $T_1 = T_2/2$ in the Markovian regime.

Dressed TLS state lines

A time segment between any two consecutive points chosen from $0, t$ or contracted interaction points in a diagram in Fig. 2.1 may be viewed as a dressed TLS line in which all possible interaction terms for the coherent state matrix element are summed. An example term is given by:

$$\int_{t_j}^{t_{2n+j+1}} dt_{2n+j} \ldots \int_{t_j}^{t_{j+3}} dt_{j+2} \int_{t_j}^{t_{j+2}} dt_{j+1} \times \langle\{\alpha\}| : A_{2n+j} A^{\dagger}_{2n+j-1} \ldots A_{j+2} A^{\dagger}_{j+1} : |\{\alpha\}\rangle \tag{2.22}$$

The normal product in the integrand enables the evaluation of the coherent state matrix element by putting the creation operator to the left with the substitution $a_k^\dagger \to \alpha_k^*$, and the annihilation operator to the right with $a_k \to \alpha_k$. The control is given by,

$$\sum_k \left(g_k e^{-i\omega_k t}\alpha_k + c.c\right) = \frac{\Omega(t)}{2} e^{-i(\omega_0 t+\phi)} + \text{c.c.}, \tag{2.23}$$

which relates α_k with the envelope function $\Omega(t)$, the resonant frequency ω_0 and the phase ϕ of the driving field. Thus, an infinite series sum of integrals like Eq. (2.22) can be carried out, leading to even and odd types of dressed photon lines (represented by Fig. 2.1(c)):

$$\begin{aligned} D_e(t,t') &= \cos\left(\frac{\mathcal{A}(t)-\mathcal{A}(t')}{2}\right)\Theta(t-t'), \\ D_o(t,t') &= (\pm)i\sin\left(\frac{\mathcal{A}(t)-\mathcal{A}(t')}{2}\right)\Theta(t-t')\ (e^{\pm i\phi}), \end{aligned} \tag{2.24}$$

corresponding, respectively, to the double and triple lines that are dressed by an even and odd number of photons in the control. Note that the dressed function $D_o(t,t')$ picks up a + (−) sign, when the triple line is on the upper (lower) time line, and gains a phase $e^{i\phi}$ ($e^{-i\phi}$), if the triple line goes from − to + in the clockwise (anticlockwise) sense. Here, $\mathcal{A}(t) = \int_0^t dt'\Omega(t')$ gives the area of the pulse at time t. In the absence of control, $D_e(t,t') \to \Theta(t-t')$ and $D_o(t,t') \to 0$, so that the double line is reduced to a single line and diagrams that contain any triple line vanish.

The mathematical expressions representing different diagrams can be obtained by first writing down all the contraction and dressed functions, and then integrating over all time variables corresponding to the vertices of each contraction line. The vertex picks up a factor of i ($-i$) if it is on the upper (lower) time line. In the following, we will provide some explicit examples.

The classical Rabi solution corresponds to diagrams with no contraction. The two dressed lines in Fig. 2.7(a) gives the transformation matrices $p_{++;++}(t)$ and $p_{-+;++}(t)$. Using Eqs. (3.9), we have

$$
\begin{aligned}
p^{(0)}_{++,++}(t) &= \cos^2\left[\frac{\mathcal{A}(t)}{2}\right], \\
p^{(0)}_{-+,++}(t) &= -ie^{i(\omega_0 t+\phi)}\cos\left[\frac{\mathcal{A}(t)}{2}\right]\sin\left[\frac{\mathcal{A}(t)}{2}\right].
\end{aligned} \tag{2.25}
$$

which is the Rabi solution without decoherence.

Vacuum relaxation of TLS

In the absence of control, the photon lines are not dressed. A broadband DOS yields the Markovian limit,

$$
K^M(t-t') = \frac{1}{T_1}\delta(t-t'). \tag{2.26}
$$

Then all the diagrams in Fig. 2.7(b) and (c) can be summed exactly, yielding respectively:

$$
\begin{aligned}
p^{vacuum,M}_{++,++}(t) &= e^{-t/T_1}, \\
p^{vacuum,M}_{-+,-+}(t) &= e^{i\omega_0 t - t/2T_1}.
\end{aligned} \tag{2.27}
$$

This Markovian limit leads to the standard result of spontaneous emission, where $T_2 = 2T_1$. This relation can also be seen from the lowest order terms in that $p^{vacuum,M}_{++,++}(t)$ contains two lowest order diagrams, while $p^{vacuum,M}_{-+,-+}(t)$ only one.

Using the same argument, for a non-Markovian system with a general DOS and the γ parameter defined in Sec. 2.3.1, we have

$$
\begin{aligned}
p^{vacuum}_{++,++}(t) &= 1-\left(\frac{t}{T_1}\right)^{\gamma}+O\left[\left(\frac{t}{T_1}\right)^{2\gamma}\right], \\
p^{vacuum}_{-+,-+}(t) &= e^{i\omega_0 t}\left\{1-\frac{1}{2}\left(\frac{t}{T_1}\right)^{\gamma}+O\left[\left(\frac{t}{T_1}\right)^{2\gamma}\right]\right\},
\end{aligned} \tag{2.28}
$$

so that $T_2 = 2^{1/\gamma}T_1$.

Exact solution to first order in contraction

Fig. 2.1(d) shows all the diagrams with one contraction with the dressed lines. By the diagrammatic rules, the transformation matrix is:

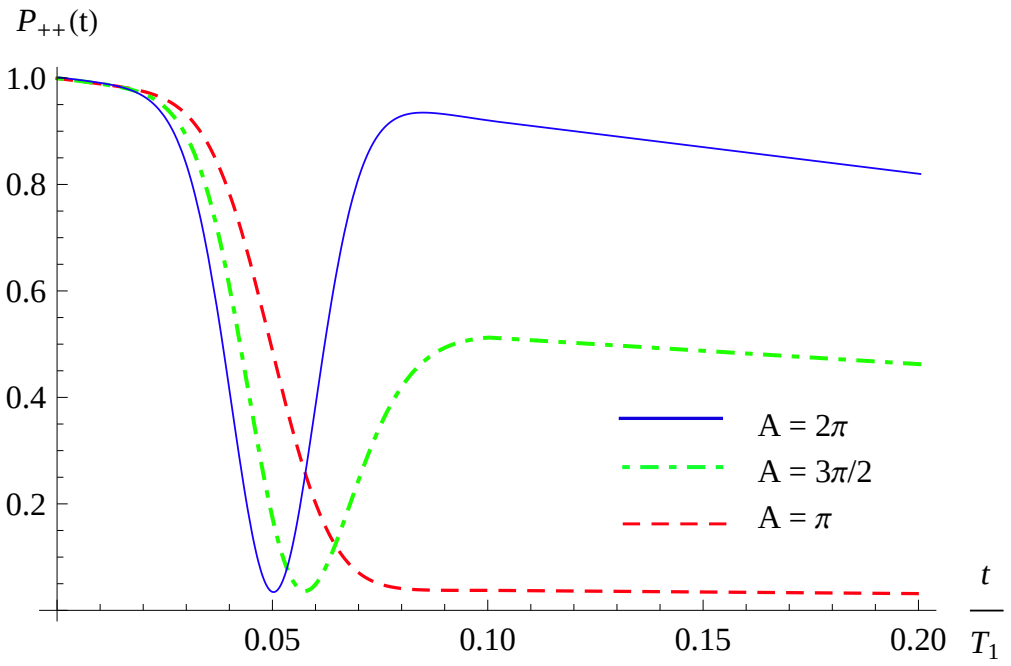

Figure 2.8: $P_{++}(t) \approx P^{(0)}_{++}(t)+P^{(1)}_{++}(t)$ of an initially excited TLS under a Gaussian pulse in the Markovian limit. It is in quantitative agreement with the optical Bloch solution.

$$p^{(1)}_{++,++}(t) = 2Z_1(t) + Z_2(t), \tag{2.29}$$

$$\text{where } Z_1(t) = -D_e(t,0)\int_0^t d\tilde{t}\int_0^{\tilde{t}} d\tilde{t}' K(\tilde{t}-\tilde{t}') \times D_e(t,\tilde{t})D_e(\tilde{t},\tilde{t}')D_e(\tilde{t}',0), \tag{2.30}$$

$$Z_2(t) = \int_0^t d\tilde{t}\int_0^t d\tilde{t}' K(\tilde{t}-\tilde{t}') \times D_o(t,\tilde{t})D_o(t,\tilde{t}')D_e(\tilde{t},0)D_e(\tilde{t}',0). \tag{2.31}$$

Z_1 and Z_2 correspond to the non-crossing and crossing diagrams respectively. This result is valid for arbitrary photon DOS and thus covers both the Markovian and non-Markovian regimes. This is the basis for the result in Sec 2.3 using a Gaussian DOS, Eq. (2.12).

The diagrammatic method can reproduce the Markovian results. By Eq. (2.26) and (2.29), Fig. 2.8 shows a Markovian example of an initially excited TLS driven by a Gaussian pulse at resonance (the same physical situation as Sec. 2.3 B).

Our result not only shows an excellent agreement with the optical Bloch analysis in this Markovian limit, but also allows an understanding of the underlying processes. For instance, the nodes of $P_{++}(t)$ do not reach zero. We note that this feature has been observed in many experiments,[24, 26, 25, 27] but cannot exclude other experimental noise sources as the cause of the feature. This theoretical feature can be understood through our diagrammatic representation in Fig. 2.1(d). One can show that the non-zero node arises from the crossing contraction term, which is very different from the vacuum decoherence that contains non-crossing contractions only (Fig. 2.7(b)).

2.7.4 Master Equation Approximations

The four approximations for the ME approach used in Sec. 3.3 are detailed here. The standard ME for the TLS up to the second Born approximation is given by (p. 250 of Ref. [28]):

$$\begin{aligned}
&\frac{d}{dt}\rho_s^{Born}(t) \\
=&-i\mathrm{Tr}_R\left[V(t),\rho_s^{Born}(0)\otimes\rho_R\right] \\
&-\int_0^t dt'\mathrm{Tr}_R\left[V(t),\left[V(t'),\rho_s^{Born}(t')\otimes\rho_R\right]\right].
\end{aligned} \tag{2.32}$$

This equation is derived from a second order expansion of the Liouville equation. In the single mode JC system, at resonance, the interaction is $V(t)=g\left(\sigma_+a+\sigma_-a^\dagger\right)$ and the reservoir density matrix constant, $\rho_R=|\alpha\rangle\langle\alpha|$.

The Nakajima-Zwanzig (NZ) and time convolutionless (TCL) projective operator techniques are outlined systematically.[20, 13] The usual assumption of $\mathrm{Tr}_R[V(t)\otimes\rho_R]$ vanishing is unnecessary and is not made in our control problem. The second order NZ ME, derived by the method of Breuer *et al.*,[20, 13] is then:

$$
\begin{aligned}
&\frac{d}{dt}\rho_s^{\mathrm{NZ}}(t) \\
=& -i\mathrm{Tr}_R\left[V(t),\rho_s^{\mathrm{NZ}}(t)\otimes\rho_R\right] \\
&+\int_0^t dt'\mathrm{Tr}_R\left[V(t),\mathrm{Tr}_R\left[V(t'),\rho_s^{\mathrm{NZ}}(t')\otimes\rho_R\right]\otimes\rho_R\right] \\
&-\int_0^t dt'\mathrm{Tr}_R\left[V(t),\left[V(t'),\rho_s^{NZ}(t')\otimes\rho_R\right]\right]. \qquad (2.33)
\end{aligned}
$$

The second order TCL ME shares the same structure but $\rho_s^{NZ}(t')$ is replaced by $\rho_s^{TCL}(t)$ in the integrand.

The additive ME assumes that the control and relaxation terms are additive (see Eq. (3.10)). In the single mode JC system, it becomes:

$$
\begin{aligned}
&\frac{d}{dt}\rho_s^{\mathrm{add}}(t) \qquad (2.34)\\
=& -ig|\alpha|[\sigma_+e^{-i\phi}+\sigma_-e^{i\phi},\rho_s^{\mathrm{add}}(t)]+g\tan gt \\
&\times\left\{2\sigma_-\rho_s^{\mathrm{add}}(t)\sigma_+-\sigma_+\sigma_-\rho_s^{\mathrm{add}}(t)-\rho_s^{\mathrm{add}}(t)\sigma_+\sigma_-\right\},
\end{aligned}
$$

where $\alpha=|\alpha|e^{i\phi}$. By neglecting the second term, the first control term leads to the classical Rabi motion. On the other hand, in the absence of the control ($|\alpha|=0$), the second term will produce the vacuum Rabi oscillations of the single mode JC system. In the small time regime ($gt\ll 1$), it corresponds to a Gaussian relaxation.

For an initially excited single mode JC system under a coherent control with a pulse are of the order of one, i.e. $\mathcal{A}=2g|\alpha|t\sim O(1)$, Eqs. (2.32-2.34) are solved and compared with the exact, the diagrammatic and the classical methods. The diagrammatic solution is calculated from Appendix 2.7.3 using the single-mode contraction function $K(t-t')=g^2$. The comparison in Sec.3.3 uses the following resultant solutions:

$$
\begin{aligned}
P_{++}^{\text{exact}}(t) &= \sum_n \cos^2\left(g\sqrt{n+1}\ t\right) \frac{|\alpha|^{2n}}{n!} e^{-|\alpha|^2}, \\
P_{++}^{\text{diagram}}(t) &= \cos^2 g|\alpha|t - \frac{(gt)^2}{4}\cos 2g|\alpha|t - \frac{3}{8}\frac{gt}{|\alpha|}\sin 2g|\alpha|t + O\left[(gt)^4\right], \\
P_{++}^{\text{classical}}(t) &= \cos^2\left(g|\alpha|t\right). \qquad (2.35)
\end{aligned}
$$

Bibliography

[1] E. T. Jaynes and F. W. Cummings, "Comparison of quantum and semiclassical radiation theories with application to the beam maser", Proc. IEEE **51**, 89, (1963).

[2] P. Aliferis, F. Brito, D. P. DiVincenzo, J. Preskill, M. Steffen and B. M. Terhal, "Fault-tolerant computing with biased-noise superconducting qubits: a case study", New J. Phys. **11**, 013061, (2009).

[3] D. Gottesman, "An Introduction to Quantum Error Correction and Fault-Tolerant Quantum Computation", e-prints arXiv:0904.2557 (2009).

[4] K. Khodjasteh and D. A. Lidar, "Fault tolerant quantum dynamical decoupling", Phys. Rev. Lett. **95**, 180501, (2005).

[5] M. Grace, C. Brif, H. Rabitz, I. A. Walmsley, R. L. Kosut and D. A. Lidar, "Optical control of quantum gates and suppression of decoherence in a system of interacting two level particles", J. Phys. B **40**, s103, (2007).

[6] J. P. Barnes and W. S. Warren, "Decoherence and programmable quantum computation", Phys. Rev. A **60**, 4363, (1999).

[7] P. R. Berman and V. S. Malinovsky, *Principles of laser spectroscopy and quantum optics* (Princeton Univ. Press, Princeton, 2011).

[8] T. Yoshie, A. Scherer, J. Hendrickson, G. Khitrova, H. M. Gibbs, G. Rupper, C. Ell, O. B. Shchekin and D. G. Deppe, "Vacuum rabi splitting with a single quantum dot in a photonic crystal nanocavity", Nature **432**, 200, (2004).

[9] P. Lodahl, A. F. van Driel, I. S. Nikolaev, A. Irman, K. Overgaag, D. Vanmaekelbergh and W. L. Vos, "Controlling the dynamics of spontaneous emission from QD by photonic crystals", Nature **430**, 654, (2004).

[10] S. Swain, "An exact solution of the multiatom, multimode model Hamiltonian of quantum optics", J. Phys. A: Gen. Phys. **5**, L3, (1972).

[11] H. J. Carmichael, *Statistical methods in quantum optics 1: Master equations and Fokker-Planck equations* (Springer, Berlin, 1999).

[12] H. M. Wiseman and G. J. Milburn, *Quantum Measurement and Control* (Cambridge University Press, Cambridge, UK, 2010).

[13] H.-P. Breuer and F. Petruccione, *Theory of Open Quantum Systems* (Oxford Univ. Press, New York, 2002).

[14] B. W. Shore and P. L. Knight, "Topical review The Jaynes Cummings Model", J. Mod. Opt. **40**, 1195, (1993).

[15] G. C. Wick, "The evaluation of the collision matrix", Phys. Rev. **80**, 268, (1950).

[16] J. C. Ward, "An identity in quantum electrodynamics", Phys. Rev. **78**, 182 (1950).

[17] G. Rempe, H. Walther and N. Klein, "Observation of quantum collapse and revival in a one atom maser", Phys. Rev. Lett. **58**, 353, (1987).

[18] D. M. Meekhof, C. Monroe, B. E. King, W. M. Itano, and D. J. Wineland, "Generation of nonclassical motional states of a trapped atom", Phys. Rev. Lett. **76**, 1796, (1996).

[19] M. Brune, F. Schmidt-Kaler, A. Maali, J. Dreyer, E. Hagley, J. M. Raimond, and S. Haroche, "Quantum Rabi Oscillation: A Direct Test of Field Quantization in a Cavity", Phys. Rev. Lett. **76**, 1800, (1996).

[20] H.-P. Breuer, B. Kappler and F. Petruccione, "Stochastic wave function method for nonMarkovian quantum master equations", Phys. Rev. A **59**, 1633, (1999).

[21] C. Gardiner and P. Zoller, *Quantum Noise: A Handbook of Markovian and Non-Markovian Quantum Stochastic Methods with Applications to Quantum Optics* (Springer, New York, 2000), p. 88.

[22] J. Gea-Banacloche, "Some implications of the quantum nature of laser fields for quantum computations", Phys. Rev. A **65**, 022308, (2002).

[23] H. Zheng, S. Y. Zhu and M. S. Zubairy, "Quantum Zeno and Anti-Zeno Effects: Without the Rotating-Wave Approximation", Phys. Rev. Lett. **101**, 200404, (2008).

[24] H. M. Gibbs, "Incoherent Resonance Fluorescence from a Rb Atomic Beam Excited by a Short Coherent Optical Pulse", Phys. Rev. A **8**, 446, (1973).

[25] F. H. L. Koppens, C. Buizert, K. J. Tielrooij, I. T. Vink, K. C. Nowack, T. Meunier, L. P. Kouwenhoven and L. M. K. Vandersypen, "Driven coherent oscillations of a single electron spin in a quantum dot", Nature **442**, 766, (2006).

[26] D. Press, T. D. Ladd, B. Zhang and Y. Yamamoto, "Complete quantum control of a single quantum dot spin using ultrafast optical pulses", Nature **456**, 218, (2008).

[27] T. H. Stievater, Xiaoqin Li, D. G. Steel, D. Gammon, D. S. Katzer, D. Park, C. Piermarocchi, and L. J. Sham, "Rabi osillations of excitions in single quantum dots", Phys. Rev. Lett. **87**, 133603, (2001).

[28] M. O. Scully and M. S. Zubairy, *Quantum Optics* (Cambridge Univ. Press, Cambridge, 1997).

Chapter 3

Quantum correlation of a quantum system driven by quantum photon controls

The controllability of a quantum system relies on an accurate account of the quantum interference among the system, the quantum control and the quantum environment. In the previous chapter, we introduce the diagrammatic technique to precisely calculate this quantum correlation for a fast multimode coherent photon control against slow relaxation, valid for both Markovian and non-Markovian photonic environment. Yet, the diagrammatic formalism is not restricted to the situation that the photon control is the coherent Glauber state. In this chapter, we extend the diagrammatic formalism and apply it to cases with controls by photon states that have more quantum mechanical nature.

3.1 Introduction

The study of an open quantum system aims at understanding the underlying physical processes between a quantum system and the environment and at giving a correct account of the system noise due to the environment. Conventional theories usually assume a weak system-environment interaction. This assumption is no longer valid for a controlled quantum system, where the control, as a

part of the environment, strongly interacts with the system. Quantum interference between the system and the control and decoherence environment can modify the noise in the quantum system. Given the recent advances in the experimental ultrafast optical techniques, an accurate theory that captures such an quantum interference effect is needed in the regime $t_0 \ll T_2$, where t_0 and T_2 are the operation and decoherence times, respectively. Also, the stringent error threshold requirement ($\epsilon \sim 10^{-4}$) demanded by fault tolerant quantum computation [1] is another motivation for a high precision theory for open quantum systems.

The master equation (ME) approach has been successful for Markovian open quantum systems [2], where the dynamics of the system is history independent. For such a Markovian system under a coherent control, the corresponding MEs are equivalent to the optical Bloch equations [3], where the control and dissipation terms are additive in the equations. However, for systems with a structured environment [4], e.g. photonic crystal materials [5] and nanocavity systems [6, 7], the dynamics are non-Markovian and the optical Bloch theory is inapplicable. In fact, because of the memory effect of these systems, interferences exist between the control and the environment and the validity of the additive form of the ME is questionable. Therefore, the challenge remains open in non-Markovian systems.

A precise diagrammatic technique has been formulated to solve the dynamics of a two level system (TLS) under a time-dependent coherent photon control through the multimode Jaynes-Cummings (JC) interaction in the regime $t_0 \ll T_2$ [8]. It takes into full account of the quantum interference among the TLS, the control and the electromagnetic vacuum and is applicable for both Markovian and non-Markovian situations. The idea is to construct the time evolution of the TLS in terms of a time loop propagation, in the same spirit as the Keldysh non-equilibrium Green's function technique [9]. Under this construction, the underlying physical processes become transparent: dissipations originate from the contraction between photons at different times; coherent Rabi motions are due to propagators dressed by the control photons; interferences between these two processes result in the control noise. For $t_0 \ll T_2$, only diagrams with a small number of contractions are important and they can be summed exactly, allowing a precise calculation of the

controlled dynamics of the TLS in this time domain within a given error bound. Based on a simple non-Markovian model, it has been shown that this diagrammatic formalism captured quantum correlations of the entire system that was missed in conventional ME approximations even in the small time limit [8]. The error of the ME approximations is comparable to that of the classical approximation.

This diagrammatic approach is not restricted to the case where the photon control is a Glauber state. The control can formally be extended to an arbitrary photon state. To illustrate this, we extend the theory to the cases of a multimode squeezed coherent state and a multimode photon number state. Comparisons with the single mode results indicate the accuracy of these diagrammatic solutions.

The chapter is organized as follows. In Section 3.2, we describe the diagrammatic formalism for a TLS under a coherent control and provide rules for the diagrammatic construction. Section 3.3 performs an explicit comparison with the standard ME approaches. We also demonstrate the ability of the diagrammatic approach to systematically improve the accuracy by including higher order diagrams. Section 3.4 extends the discussion to non-Glauber photon controls. We conclude in Section 3.5.

3.2 TLS under coherent control

The central idea of the diagrammatic technique is first to express the time evolution of the composite system in terms of the spin and photon operators, then to evaluate the transition matrix in terms of photon operators, which are finally treated diagrammatically using the Wick's expansion. The problem of a time-dependent controlled TLS is governed by the multimode JC Hamiltonian under a multimode coherent state $|\boldsymbol{\alpha}\rangle = |\alpha_{k_1}, \alpha_{k_2}, \ldots\rangle$. Consider first for simplicity, an initial wavefunction of the product form $|\Psi(0)\rangle = [\sum_s c_s|s\rangle]\,|\boldsymbol{\alpha}\rangle$, where $s = \pm$ gives the spin state. The system evolves as $|\Psi(t)\rangle = U(t)|\Psi(0)\rangle$, where the evolution operator in the interaction picture is given by:

$$U(t) \;=\; T\exp\Big[-i\int_0^t dt' V(t')\Big], \tag{3.1}$$

and the multimode JC interaction is:

$$V(t_l) = \sigma_+ A_l + \sigma_- A_l^\dagger, \tag{3.2}$$

$$\text{with } A_l = \sum_k g_k a_k e^{i(\omega_0-\omega_k)t_l}. \tag{3.3}$$

with ω_0 the energy splitting of the TLS, ω_k the photon frequency and g_k the TLS-photon coupling strength. The interaction on the initial coherent photon state can be viewed as the action of a control pulse, consisting of a modulation of the resonant frequency mode with the coherent state amplitude satisfying:

$$\sum_k \left(g_k e^{-i\omega_k t}\alpha_k + c.c\right) = \frac{\Omega(t)}{2} e^{-i(\omega_0 t+\phi)} + \text{c.c.}, \tag{3.4}$$

where α_k is the eigenvalue of a_k on $|\boldsymbol{\alpha}\rangle$, $\Omega(t)$ and ϕ are the envelope function and phase of the pulse, respectively. Note that we have made the rotating wave approximation which is valid when $\omega_0 t \gg g|\alpha|t \sim O(1)$ [8]. The physical quantity of interest is the transformation matrix:

$$\begin{aligned} p_{s_f,s_f';s,s'}(t,\boldsymbol{\alpha}) &= \langle\boldsymbol{\alpha}|\langle s'|U^\dagger(t)|s_f'\rangle\langle s_f|U(t)|s\rangle|\boldsymbol{\alpha}\rangle \\ &\quad \times e^{i(s_f' 1 - s_f 1)\omega_0 t/2}, \end{aligned} \tag{3.5}$$

from which we can obtain the reduced density matrix of the TLS at that:

$$P_{s_f,s_f'}(t) = \sum_{s,s'} c_s c_{s'}^* p_{s_f,s_f';s,s'}(t,\boldsymbol{\alpha}). \tag{3.6}$$

It is straightforward to generalize the above formulae to an initial state which is a linear combination of the product states.

In contrast to the ME methodology which traces out the photonic environment in the beginning, we evaluate the TLS transition by the spin operators in the transformation matrix first, leaving a sequence of the corresponding photon components. An example is given by:

$$\begin{aligned} & p_{++;++}(t) \\ = & \sum_{n,n'=0}^{\infty} (-1)^{n+n'} \int_0^t D^{2n}t \int_0^t D^{2n'}t \\ \times & \langle\boldsymbol{\alpha}| \left(A_{1'}A_{2'}^\dagger ... A_{2n'-1}A_{2n'}^\dagger\right)\left(A_{2n}A_{2n-1}^\dagger ... A_2 A_1^\dagger\right)|\boldsymbol{\alpha}\rangle\,, \end{aligned} \tag{3.7}$$

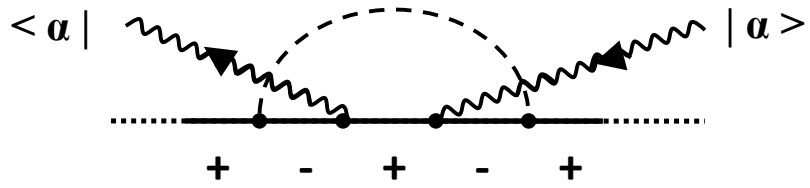

Figure 3.1: An illustration of the TLS-multiphoton process conditioned on a multimode coherent state. The ± sign labels the spin state of the TLS. Contractions among photons (dashed line) correspond to decoherence, while the normal-ordered control photons (wavy lines) is responsible for the Rabi motion of the TLS.

where $\int_0^t D^n t = \int_0^t dt_n ... \int_0^{t_3} dt_2 \int_0^{t_2} dt_1$. In the following, we will focus on this expression for illustration. Other transformation matrices can be obtained similarly (see [8]). Therefore, the task is now reduced to compute expectation values of the photon operators for the initial multimode coherent state.

Eq. (3.7) is exact up to now and all the quantum correlations of the whole system remain intact. The underlying physical processes can be easily identified using a diagrammatic representation as in Fig. 3.1. We shall see in the next subsection how different roles of the photons affect the interaction dynamics, and how this infinite series expression can be largely simplified and summed to a desirable accuracy using t/T_2 as a small parameter. No stochastic assumption has been made. We emphasize that this approach is fundamentally different from the ME method which usually assumes a stationary environment and thus does not account for the interference effect between the control and the environment of a quantum system.

3.2.1 Diagrammatic solution

It is instructive to describe Eq. (3.7) as time loop integrals of photon operators propagating forward and backward between time 0 and t, and depict Fig. 3.1 in a bubble form. Diagrammatic series is constructed using the Wick's theorem [10], which expands the product of photon operators in terms of the normal ordered

form and possible contractions between two photon operators. By doing so, the expectation value in Eq. (3.7) can be computed easily by the replacement $a_k \to \alpha_k$ and $a_k^\dagger \to \alpha_k^*$ for normal ordered photons. Physically, the normal ordered photons coming from the multimode coherent state are responsible for the coherent Rabi motion of the TLS; while the contraction between photons, being independent of the control, corresponds to vacuum relaxation of the TLS.

The diagrammatic structure consists of two ingredients: the contraction between photons and dressed lines due to the coherent control. The contraction function is given by:

$$\langle A_i A_j^\dagger \rangle \;=\; K(t_i - t_j) = \sum_k g_k^2 e^{i(\omega_0 - \omega_k)(t_i - t_j)}, \tag{3.8}$$

and is depicted in Fig. 3.2a. Here, t_i and t_j can be on the same or opposite time lines. Note that the contraction only depends on the photon density of state (DOS) $\rho(\omega) = \sum_k g_k^2 \delta(\omega - \omega_k)$. One can show that each contraction line $\sim \int\int dt_i dt_j K(t_i - t_j) \sim O[(t/T_2)^\gamma]$, where $1 \le \gamma \le 2$ depends on the DOS [8]. Therefore, the Wick's expansion in terms of contraction is automatically a perturbative series of the small parameter $(t/T_2)^\gamma$. On the other hand, the dressed lines lead to Rabi oscillations of the TLS and are given by [8]:

$$\begin{aligned} D_e(t,t') &= \cos\left(\frac{\mathcal{A}(t) - \mathcal{A}(t')}{2}\right)\Theta(t-t'), \\ D_o(t,t') &= (\pm i)(e^{\pm i\phi}) \sin\left(\frac{\mathcal{A}(t) - \mathcal{A}(t')}{2}\right)\Theta(t-t'), \end{aligned} \tag{3.9}$$

corresponding to the double and triple line depicted in Fig. 3.2b. A dressed line segment between the same (opposite) spin state corresponds to a double (triple) line. Here, $D_o(t,t')$ picks the factor $+i$ $(-i)$, when the triple line is on the upper (lower) time line; and gains a phase $e^{i\phi}$ $(e^{-i\phi})$, if it goes from $-$ to $+$ in the clockwise (anticlockwise) sense. $\mathcal{A}(t) = \int_0^{t'} dt' \Omega(t')$ gives the area of the coherent pulse at time t. Physically, $D_e(t)$ and $D_o(t)$ are just the diagonal and off-diagonal matrix elements of the 2 by 2 propagators of a TLS under a coherent control.

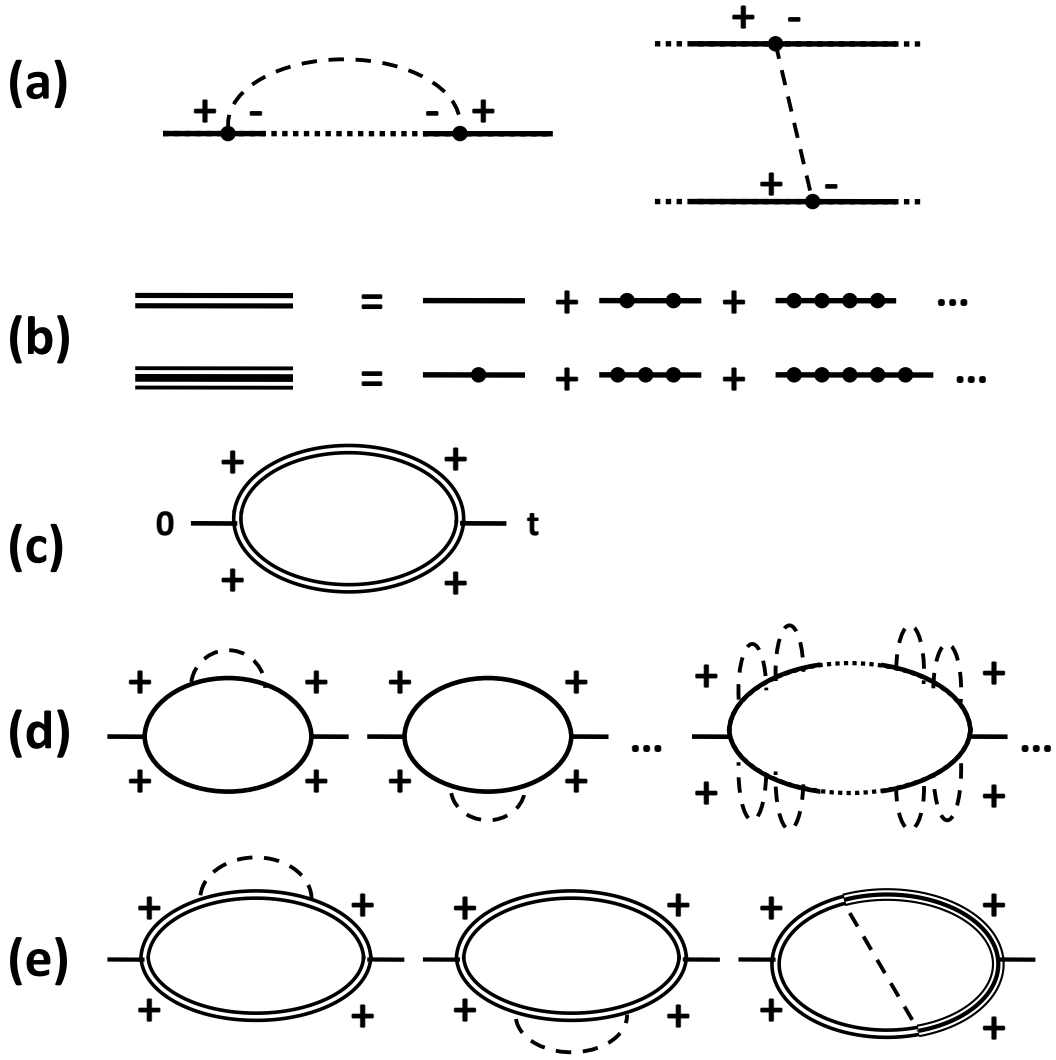

Figure 3.2: Diagrammatic representations of the Wick's expansion of the transformation matrix $p_{s_f,s'_f;s,s'}(t,\{\alpha\})$ for a general photonic control. (a) The two possible contractions between photons at different times. (b) Two types of dressed line that represent a sum of even or odd numbers of control photons interacting with the TLS. (c) A dressed diagram without any contraction represents the driven oscillations of the two state system from time 0 to t. (d) Vacuum relaxation is represented by undressed diagrams with contractions only. (e) The leading contribution of control noise to $p_{++;++}$ comes from three dressed diagrams with only one contraction.

The diagrammatic procedure can be summarized as follows: (i) denote the initial and final state of the transformation matrix on a loop diagram, where the lower and upper arcs represent forward and backward time evolutions; (ii) draw all possible contractions according to Fig. 3.2a; and (iii) dress the bare lines according to the spin flips by the photons. Each diagram can be computed straightforwardly by integrating over all time variables at the vertices of each contraction line. The vertex picks up a factor of i $(-i)$ when it is on the upper (lower) time line.

The diagrammatic structure allows an easy identification of the underlying coherent and dissipative processes. For instance, Fig. 3.2c shows the diagram with no contraction but infinite series of coherent photons for $p_{++;++}(t)$. Following the above description, this uninterrupted diagram simply gives the expected coherent Rabi solution $p^{(0)}_{++;++}(t) = \cos^2[\mathcal{A}(t)/2]$. On the other hand, in the absence of control, the vacuum relaxation is represented by a series of undressed diagrams that involves contractions only, as can be seen in Fig. 3.2d. In the regime $t \ll T_2$, the first two diagrams in Fig. 3.2d results in a decoherence of $\sim O[(t/T_2)^\gamma]$.

One advantage of the diagrammatic method is that summing infinite subseries of diagrams is feasible. Fig. 3.2e shows the leading order diagrams for the control noise problem. Interference between the control (dressed line) and decoherence (contraction line) is evident. We stress that these diagrams are first order in decoherence, but infinite order in the coherent interaction. This explains why the diagrammatic approach is a suitable candidate to our control noise problem, in contrast to the ME method that requires a weak system-environment coupling.

3.2.2 Application to a general DOS

The field theoretic approach described above is applicable for an arbitrary photon DOS and thus valid for both the Markovian and non-Markovian systems. For a broadband DOS, the contraction function becomes a delta function $K(t_i - t_j) \sim \delta(t_i - t_j)$, meaning that the two ends of a contraction line are squeezed to the same point. In this limit, the correlation time τ_c is zero and the decoherence is linear in t/T_2 (i.e. $\gamma = 1$), corresponding to a Markovian exponential decay. The dynamics of the controlled TLS can be alternatively obtained by the optical Bloch

equation and the diagrammatic solution shows quantitative agreement with it in the regime $t \ll T_2$ [8].

Extension to the non-Markovian regime can be performed simply by modifying the photon DOS and thus the contraction function. The correlation time τ_c is characterized by the bandwidth of the DOS. The contraction function is no longer a delta function, leading to non-exponential decoherence $\sim O[(t/T_2)^\gamma]$, where $1 < \gamma \leq 2$. Furthermore, there is a transition from the non-exponential to exponential decay as t becomes comparable to τ_c. All these features remain in the presence of a coherent control [8]. In the following section, we will investigate the accuracy of the diagrammatic scheme in comparison with existing ME methods.

3.3 Comparison with ME approaches

Conventional master equation (ME) assumes an additive form [11]:

$$\frac{d}{dt}\rho_s(t) = -i[H_c(t), \rho_s(t)] + \int_0^t dt' \hat{L}(t-t')\rho_s(t'), \tag{3.10}$$

where $H_c(t)$ describes a control Hamiltonian that only acts on the system and $\hat{L}(t-t')$ is a suitably chosen superoperator that only accounts for the dissipative environment. It is assumed that these two terms are independent on each other. In this section, we examine the validity of this kind of ME against the field theoretic solution in Section 3.2.

3.3.1 Second order TLS-environment interaction

We consider two commonly adopted ME approaches based on the projective operator techniques, namely the Nakajima-Zwanzig (NZ) and the time-convolutionless (TCL) methods [12, 13]. We now show that they belong to the

additive ME in Eq. (3.10). The second order NZ ME is given by:

$$\begin{aligned}
&\frac{d}{dt}\rho_s^{\mathrm{NZ}}(t) \\
= \;& -i\mathrm{Tr}_R\left[V(t), \rho_s^{\mathrm{NZ}}(t)\otimes\rho_R\right] \\
&+ \int_0^t dt' \mathrm{Tr}_R\left[V(t), \mathrm{Tr}_R\left[V(t'), \rho_s^{\mathrm{NZ}}(t')\otimes\rho_R\right]\otimes\rho_R\right] \\
&- \int_0^t dt' \mathrm{Tr}_R\left[V(t), \left[V(t'), \rho_s^{NZ}(t')\otimes\rho_R\right]\right], \qquad (3.11)
\end{aligned}$$

where $\rho_s(t)$ is the reduced density matrix of the TLS, $\rho_R = |\boldsymbol{\alpha}\rangle\langle\boldsymbol{\alpha}|$ denotes the initial multimode photon density matrix and has no time dependence. The non-vanishing first and second terms are due to fact that $\mathrm{Tr}_R[V(t)\otimes\rho_R] \neq 0$. Using the multimode JC interaction in Eq. (3.1) and the relation in Eq. (3.4), we trace out the photon reservoir and arrive at the NZ ME:

$$\begin{aligned}
&\frac{d}{dt}\rho_s^{\mathrm{NZ}}(t) \\
= \;& -i\frac{\Omega(t)}{2}\left[\sigma_+ e^{i\phi} + \sigma_- e^{-i\phi}, \rho_s^{\mathrm{NZ}}(t)\right] \\
&- \int_0^t dt' K(t-t')\left[\sigma_+\sigma_-\rho_s^{\mathrm{NZ}}(t') - \sigma_-\rho_s^{\mathrm{NZ}}(t')\sigma_+ + h.c.\right], \\
& \qquad (3.12)
\end{aligned}$$

where $K(t-t')$ is just the contraction function in Eq. (3.8). The second order TCL ME can be obtained simply by the replacement $\rho_s^{TCL}(t') \to \rho_s^{TCL}(t)$ in the integrand.

It is clear from Eq. (3.12) that the NZ ME and TCL ME belong to the class of additive ME in Eq. (3.10), where the corresponding superoperators $\hat{L}(t-t')$ do not depend on the control, and thus both of them have neglected the quantum interference effect between the control and dissipation. This can be explicitly illustrated by using a simple non-Markovian system, the single mode JC model, where an exact solution is available. This situation corresponds to a constant contraction function $K(t-t') = g^2$, infinite correlation time $\tau_c = \infty$, $\gamma = 2$ and $T_2 = \sqrt{2}/g$. We consider an initially excited TLS under a single mode coherent drive with $\bar{n} = 100\pi^2$, so that the system undergoes a 4π rotation when $gt = 0.2$. Fig. 3.3 compares the difference between different approaches and the exact

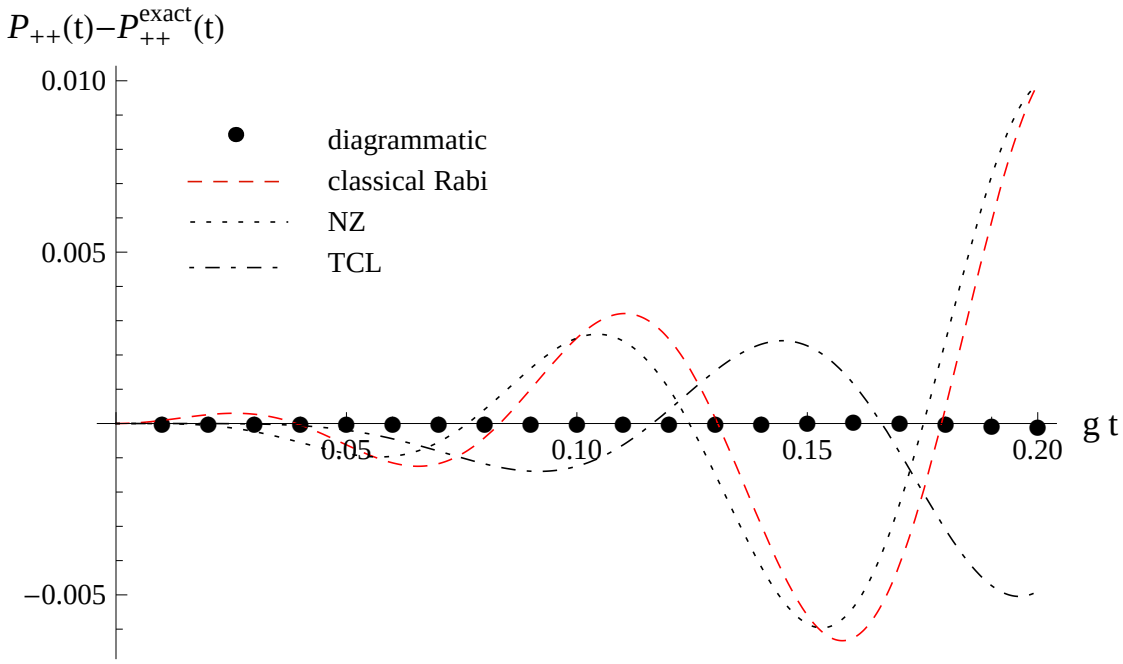

Figure 3.3: A comparison between the diagrammatic methods and the ME approaches using a coherently driven single mode JC system with $\bar{n} = 100\pi^2$, corresponding to a 4π rotation at $gt = 0.2$. The magnitudes of errors of the ME approaches and the classical Rabi solution are comparable even in the small time regime.

solution for $P_{++}(t) = p_{++;++}(t)$. Here, the diagrammatic solution, based on the three diagrams in Fig. 3.2e, shows an excellent agreement with the exact solution in the small gt regime. The error of these three diagrams is $O[(gt)^4]$. On the contrary, these two ME methods, expected to be the same and accurate to the second order of gt [12, 13], show errors of the same order of magnitude. The error of the NZ solution is very close to that of the classical Rabi solution ($P_{++}(t) = \cos^2(g\sqrt{\bar{n}}t)$) which entirely neglects any decoherence effect; while the error of TCL result shows a phase difference from the NZ and classical solution because of the approximation $\rho_s^{TCL}(t') \to \rho_s^{TCL}(t)$ in the integrand of the ME.

The problem of these ME approximations stem from the assumptions of a stationary environment, which is inappropriate for a quantum system under a general control. Quantum feedback from the photon environment to the TLS exists and originates from the quantum interference between the control and the

environment. In fact, the difference between the field theoretic solution and the additive ME method can be viewed as the difference between the quantum and semiclassical correlations. This difference is not limited to the single mode test above and occurs for a general non-Markovian multimode system.

3.3.2 Higher order terms

The precision of the diagrammatic solution can be further improved by including higher order diagrams. In general, the inclusion of diagrams with n contractions would result in an error of $O[(t/T_2)^{(n+1)\gamma}]$. Fig. 3.4 provides the next order diagrams that possess two contractions for $p_{++;++}(t)$. They can be evaluated by using the same procedure described in Section 3.2.1. As an example, Fig. 3.5 plots the absolute difference of $P_{++}(t)$ between different methods and the exact solution in log scale under the same physical situation as in Fig. 3.3. It is apparent that the diagrammatic solution has a well-controlled error bound in the small time domain.

3.4 Control by photon states other than coherent state

The field theoretic technique can be formulated similarly when the TLS is initially in the presence of a quantum photon state other than the coherent state. The Wick's expansion is still valid, though the diagrammatic rules have to be modified. Here, we extend this formalism to the multimode squeezed coherent state and the multimode photon number state. Rather than exploring all possible scenarios, the purpose of this section is to demonstrate how diagrammatic solutions can be constructed with different initial photon states.

3.4.1 Squeezed coherent state

A multimode squeezed coherent state takes the form $|\boldsymbol{\alpha}, \xi\rangle = D(\boldsymbol{\alpha})S(\xi)\,|0\rangle$, where $D(\boldsymbol{\alpha})$ is the multimode displacement operator and we take the multimode

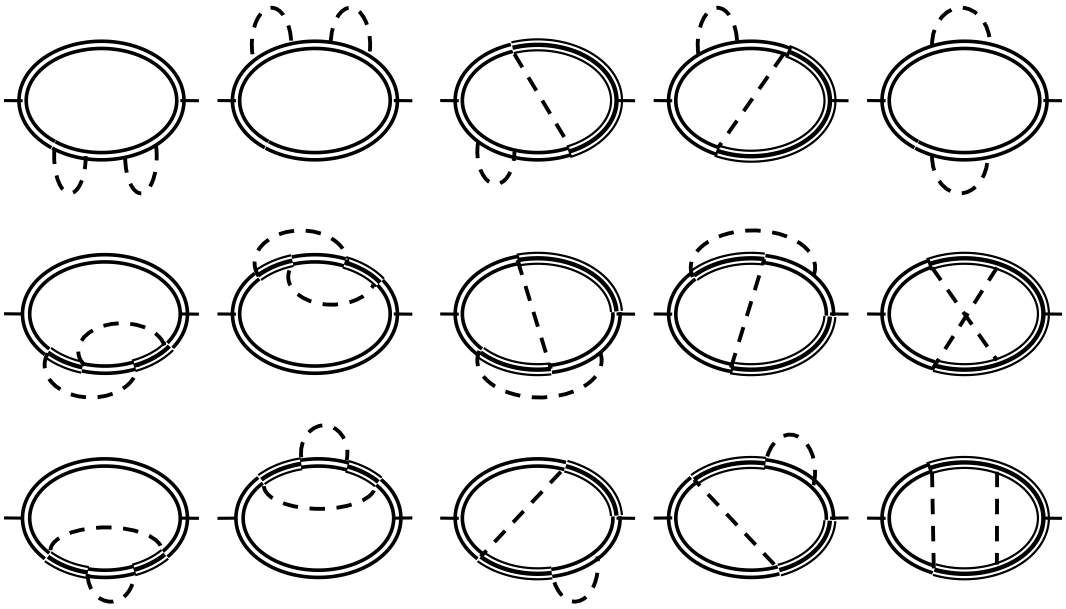

Figure 3.4: Fifteen dressed diagrams with two contractions for $p_{++;++}$ under a coherent control.

squeezing operator to be $S = \prod_k \exp\left(\xi^* a_{\bar{k}+k} a_{\bar{k}-k} - \xi a^\dagger_{\bar{k}+k} a^\dagger_{\bar{k}-k}\right)$ [14]. $\bar{k}$ governs on the squeezing mechanism. The problem is to evaluate Eq. (3.7) using $|\boldsymbol{\alpha}, \xi\rangle$ instead of $|\boldsymbol{\alpha}\rangle$.

Making use of the squeezing transformation, we can rewrite Eq. (3.7) by the replacement $A_i \to \tilde{A}_i = S^\dagger A_i S$, $A_j^\dagger \to \tilde{A}_j^\dagger = S^\dagger A_j^\dagger S$ and $D(\boldsymbol{\alpha}) \to \tilde{D}(\boldsymbol{\alpha}) = S^\dagger D(\boldsymbol{\alpha}) S$, where each photon operator transforms according to

$$\begin{aligned} S^\dagger a_k S &= a_k \cosh r - a^\dagger_{2\bar{k}-k} e^{i\theta} \sinh r, \\ S^\dagger a_k^\dagger S &= a_k^\dagger \cosh r - a_{2\bar{k}-k} e^{-i\theta} \sinh r, \end{aligned} \tag{3.13}$$

and the squeezing parameters satisfy $\xi = re^{i\theta}$. Now, we can proceed the Wick's expansion as in Section 3.2.1. The dressed lines are unaffected as the normal ordered photon operators are just c-numbers. As such, the zeroth order diagram remains the same. However, four types of contractions are now possible due to the

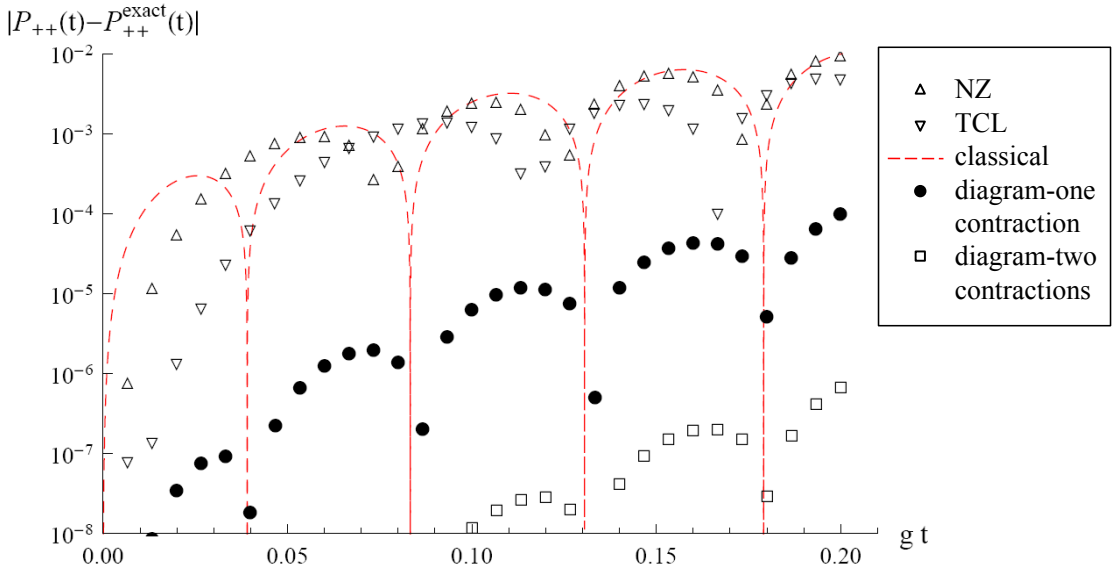

Figure 3.5: A plot of absolute errors of different methods under the same physical situation as in Fig. 3.3. Diagrammatic solution with n contractions has an error of $O\left[(gt)^{2(n+1)}\right]$.

squeezing:

$$\begin{aligned}
\langle \tilde{A}_i \tilde{A}_j^\dagger \rangle &= \cosh^2 r \sum_k g_k^2 e^{i(\omega_0-\omega_k)(t_i-t_j)}, \\
\langle \tilde{A}_i^\dagger \tilde{A}_j \rangle &= \sinh^2 r \sum_k g_k^2 e^{-i(\omega_0-\omega_k)(t_i-t_j)}, \\
\langle \tilde{A}_i \tilde{A}_j \rangle &= -\frac{e^{i\theta}}{2} \sinh(2r) \\
&\quad \times \sum_k g_k g_{2\bar{k}-k} e^{i(\omega_0-\omega_k)t_i} e^{i(\omega_0-\omega_{2\bar{k}-k})t_j}, \\
\langle \tilde{A}_i^\dagger \tilde{A}_j^\dagger \rangle &= \langle \tilde{A}_i \tilde{A}_j \rangle^*, \qquad (3.14)
\end{aligned}$$

and they are depicted in Fig. 3.6. The above dependence of the contraction functions on the squeezing parameter θ shows a phase sensitive decoherence of the TLS.

In brief, the diagrammatic rules in Section 3.2.1 still apply with the exception that the construction of contractions in Fig. 3.2a is replaced by that in Fig. 3.6. The leading order contribution to control noise now consists of twelve

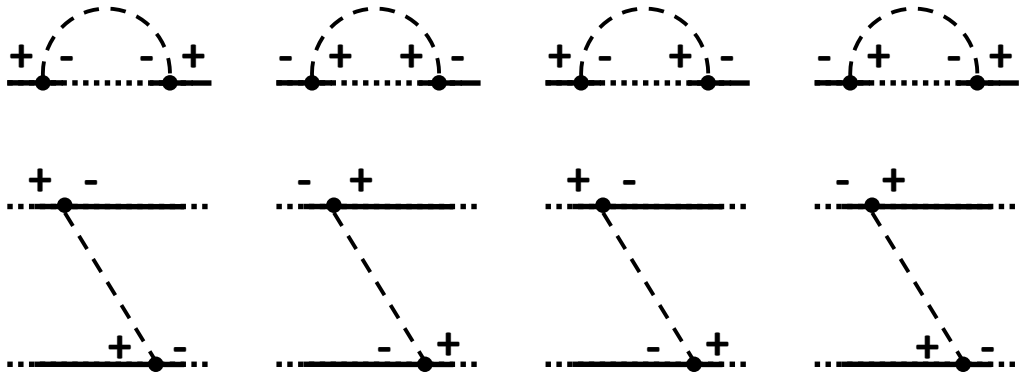

Figure 3.6: Eight possible contractions between photons for a squeezed vacuum.

diagrams which are similar to the three shown in Fig. 3.2e. To demonstrate the accuracy of the diagrammatic solution, we compare it with an exact solution of a single mode JC system under a squeezed coherent state [15]. Fig. 3.7 again shows an excellent precision of the diagrammatic solution. Depending on the squeezing parameters, the phase sensitive decoherence of the TLS can be greater or smaller than that without squeezing. We note that since the decoherence time is modified to $\sim 1/(g\cosh r)$, the small time requirement becomes $g\cosh(r)t \ll 1$ for the validity of the perturbative solution.

The above squeezed state analysis works similarly for the more general linearly transformed coherent state $D(\boldsymbol{\alpha})T\,|0\rangle$, where T is any unitary operator that transforms the photon operators linearly, $T^{\dagger}a_k T = \sum_{k'}\left(u_{kk'}a_{k'} + v_{kk'}a^{\dagger}_{k'}\right)$. The diagrammatic solution shows that the coherent motion of the TLS remains the same, while the decoherence can be computed straightforwardly by using the modified contraction functions similar to Eq. (3.14).

3.4.2 Number state

The dynamics between a TLS and a multimode number state is more complicated. A single photon process can project the photon state to be orthogonal to the initial state. It is a daunting task to keep track of the time evolution of a number state with an arbitrary photon number distribution. With the help of the

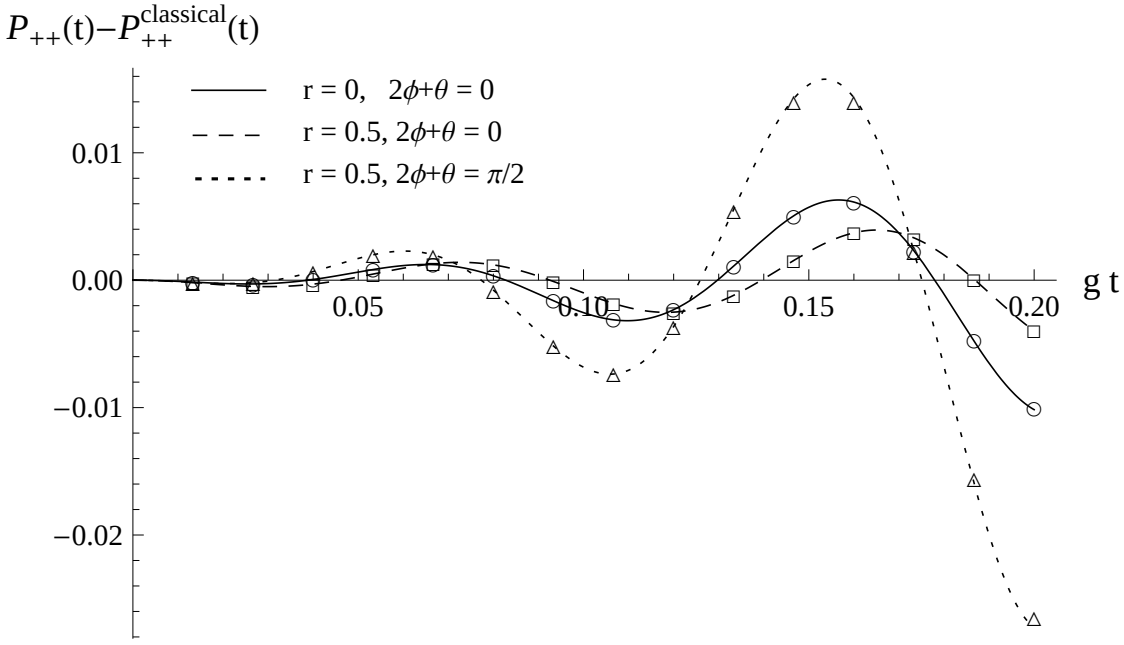

Figure 3.7: $P_{++}(t) - P_{++}^{\text{classical}}(t)$ of an initially exited TLS under a single mode squeezed coherent state with $\bar{n} = 100\pi^2$ for various squeezing parameters. ϕ is the phase of α^* and θ is the phase of squeezing. The curves and symbols correspond to the diagrammatic and exact solutions, respectively.

diagrammatic technique, we shall see below how it is possible to tackle a number state of the form $|N, \{0\}\rangle$, where $\{0\}$ is a multimode vacuum.

The idea is again to make use of the Wick's expansion of the photon operators in Eq. (3.7), where the coherent state is replaced by $|N, \{0\}\rangle$ here. We assume the N-mode of the number state has zero detuning. The zeroth order term has all the photon operators being normal ordered, so that each photon operator can only annihilate or create photons in the N-mode. Thus, the time integrals in Eq. (3.7) can be performed and the resultant expression is:

$$\begin{aligned} p^{(0)}_{++;++}(t) &= 1 - N(gt)^2 + \sum_{n,n'=1}^{\infty} (-1)^{n+n'} \frac{(gt)^{2n+2n'}}{(2n)!(2n')!} \\ &\quad \times N(N-1)...(N-n-n'+1), \end{aligned} \tag{3.15}$$

which is already different from the classical Rabi solution. The coherent photon dressing described in Section 3.2.1 no longer applies and one has to perform an infinite sum as in Eq. (3.15).

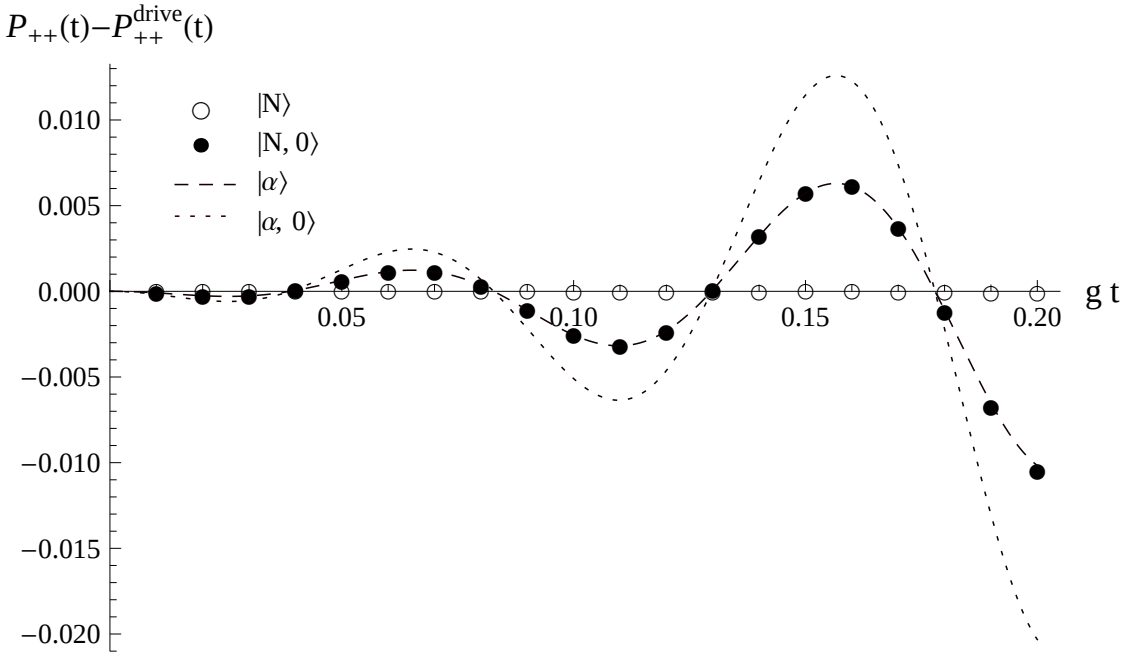

Figure 3.8: Relaxation of an initially excited TLS under different initial photon states. $N = |\alpha|^2 = 10^3$. The case with a non-dissipative single mode number state ($|N\rangle$) gains decoherence when a degenerate vacuum mode is added ($|N, 0\rangle$). In the small time region, the amount of dissipation is the same as that of a single mode coherent state ($|\alpha\rangle$).

The contraction line remains as a good small parameter. The first contraction terms can be calculated as in the way to obtain Eq. (3.15). Fig. 3.8 shows the relaxation, defined by $P_{++}(t) - P_{++}^{\text{drive}(t)}$, of a TLS driven by different initial photon states. For simplicity, we consider the vacuum mode to be degenerate with the N-mode, so that the contraction function is time independent. We define the driving term $P_{++}^{\text{drive}}(t) = \cos^2(g\sqrt{N+1}\, t)$ and $\cos^2(g|\alpha|t)$ for the number and coherent states, respectively. In the case of a single mode number state $|N\rangle$, no relaxation is seen as expected. However, when we consider a number state with one degenerate vacuum mode $|N, 0\rangle$, dissipation is observed due to the interference between the control photon and the vacuum. The amount of decoherence increases linearly with the number of degenerate vacuum modes present. It is also interesting to observe that the decoherence of $|N, 0\rangle$ is equal to that of a single mode coherent state $|\alpha\rangle$ in the small time regime.

The diagrammatic approach serves as a first step towards a precise treat-

ment of this multimode number state problem. The generalization to deal with states having a general photon number distribution remains as a challenge. The ME approximation schemes are even worse at accounting for the decoherence effect of this problem compared to their efficiencies in coherent state case. Following the discussion in Section 3.3, one can show that for an initial photon state $|N, 0\rangle$, the NZ ME leads to a non-dissipative oscillations of the TLS, where $P_{++}(t)$ can be negative even in the small time regime $gt \ll 1$. The TCL ME results in a Gaussian decay ($P_{++}^{TCL}(t) \approx [1 + \exp(-2Ng^2t^2)]/2$, for $N \gg 1$), where the Rabi oscillations are lost. Their failures again originate from the inability to capture the coupled dynamics between the control and the environment.

3.5 Summary

The diagrammatic formalism provides a new platform to understand and compute the interaction dynamics among the quantum system, the control photon and the environment. Its high accuracy is attributed by the full account of the unitary evolution of the wavefunction of the whole system without any stochastic assumption. The revelation of underlying physical processes by the diagrammatic structures enables a perturbative computation scheme for systems under fast photon control versus slow relaxation, with well-defined error bounds. It also serves as an extension of the standard field theoretic techniques in quantum electrodynamics and many-body problems to systems far from equilibrium.

The ME approach has been a good phenomenology to provide qualitative understandings of open quantum systems. Given the recent advances in high precision quantum technologies, there is a need to reexamine and improve the accuracies of the existing theories. The diagrammatic solution indicates the absence of quantum interference between the control and the environment in current ME approximations. This general effect is not restricted to a TLS interacting with a single mode photon state. We believe that the diagrammatic results can motivate improvements of conventional ME studies and stimulate the developments of other novel quantum theories. There is hope that more quantum mechanical effects of

open quantum systems will be uncovered in the future.

3.6 Acknowledgments

This research was supported by the U.S. Army Research Office MURI award W911NF0910406.

The text in chapter 3, in part, is a reprint of the material as it appears in Ching-Kit Chan and L. J. Sham, "Quantum correlation of an optically controlled quantum system", Journal of the Optical Society of America B, Feature issue,**29**, A25, (2012). The dissertation author was the first author of the paper and the co-author in this publication directed, supervised, and co-worked on the research which forms the basis of this chapter.

Bibliography

[1] P. Aliferis, F. Brito, D. P. DiVincenzo, J. Preskill, M. Steffen and B. M. Terhal, "Fault-tolerant computing with biased-noise superconducting qubits: a case study", New J. Phys. **11**, 013061 (2009).

[2] C. Gardiner and P. Zoller, *Quantum Noise: A Handbook of Markovian and Non-Markovian Quantum Stochastic Methods with Applications to Quantum Optics* (Springer, New York, 2000).

[3] P. R. Berman and V. S. Malinovsky, *Principles of laser spectroscopy and quantum optics* (Princeton Univ. Press, Princeton, 2011).

[4] P. Lambropoulos, G. M. Nikolopoulos, T. R. Nielsen and S. Bay, "Fundamental quantum optics in structured reservoirs", Rep. Prog. Phys. **63**, 455-503 (2000).

[5] P. Lodahl, A. F. van Driel, I. S. Nikolaev, A. Irman, K. Overgaag, D. Vanmaekelbergh and W. L. Vos, "Controlling the dynamics of spontaneous emission from quantum dots by photonic crystals", Nature **430**, 654-657 (2004).

[6] S. Noda, A. Chutinan and M. Imada, "Trapping and emission of photons by a single defect in a photonic bandgap structure", Nature **407**, 608-610 (2000).

[7] T. Yoshie, A. Scherer, J. Hendrickson, G. Khitrova, H. M. Gibbs, G. Rupper, C. Ell, O. B. Shchekin and D. G. Deppe, "Vacuum Rabi splitting with a single quantum dot in a photonic crystal nanocavity", Nature **432**, 200-203 (2004).

[8] C. K. Chan and L. J. Sham, "Precision of electromagnetic control of a quantum system", Phys. Rev. A **84**, 032116 (2011).

[9] L. V. Keldysh, "Diagram technique for non-equilibrium processes", JETP **20**, 1018-1027 (1965).

[10] G. C. Wick, "The evaluation of the collision matrix", Phys. Rev. **80**, 268-272 (1950).

[11] G. A. Prataviera, S. S. Mizrahi, V. V. Dodonov and J. R. Brinati, "Probing colored noise from the index of refraction of strongly driven two-level atoms", Phys. Rev. A **60**, 4045-4051 (1999).

[12] H.-P. Breuer, B. Kappler and F. Petruccione, "Stochastic wave-function method for non-Markovian quantum master equations", Phys. Rev. A **59**, 1633-1643 (1999).

[13] H.-P. Breuer and F. Petruccione, *Theory of Open Quantum Systems* (Oxford Univ. Press, New York, 2002).

[14] M. O. Scully and M. S. Zubairy, *Quantum Optics* (Cambridge Univ. Press, Cambridge, 1997).

[15] G. J. Milburn, "Interaction of a two-level atom with squeezed light", Optica Acta **31**, 671-679 (1984).

Chapter 4

Robust distant-entanglement generation using coherent multiphoton scattering

In this chapter, we describe a protocol to entangle two qubits at a distance by using resonance fluorescence. The scheme makes use of the postselection of large and distinguishable fluorescence signals corresponding to entangled and unentangled qubit states, and has the merits of both high success probability and high entanglement fidelity owing to the multiphoton nature. Our result shows that the fluorescence statistics are, respectively, sub-poissonian and super-poissonian for entangled and unentangled pairs of electronic spin, and do not affect the robustness of entanglement generation. Based on current experimental efficiencies of photon collection and detection, we demonstrate that this new protocol has an average entanglement duration within the decoherence time of corresponding qubit systems.

4.1 Introduction

The generation and controllability of entanglement between distant quantum states have been the heart of quantum computation and quantum information processing. Since the early proposal of entanglement generation in atomic ensemble

systems [1], many theoretical ideas have been put forward [2, 3, 4, 5] and experimental demonstrations of distant entanglement have been recently performed in trapped ion systems [6, 7, 8], with an average entanglement fidelity being up to 90%. These existing approaches to generate entanglement is based on postselection using single-photon measurement [1, 2, 3], and have the merit of high fidelity entanglement creation. However, due to the inefficiency of single-photon detection, these protocols have a rather low success probability in practice ($\sim$ twenty billionth in trapped ion experiments [5]). This limitation leads to the average entanglement time being longer than the decoherence time of the qubit. To counter this difficult, much experimental effort has been devoted to improve the single-photon collection efficiency in various qubit systems [9, 10, 11].

Alternative theoretical proposals to generate entanglement make use of Raman transitions of qubit systems embedded in a cavity [12, 13]. This scheme utilizes bright coherent light and thus is expected to be more efficient than the single-photon protocols, but at the expense of a moderate entanglement fidelity due to the cavity loss and spontaneous emission. Solution to overcome the sensitivity to spontaneous emission has been suggested replacing the coherent input light by either the Fock or the NOON states [14], which is experimentally more demanding. Therefore, there exists a dichotomy in the architecture of entanglement generation that is either based on a low rate, high fidelity single-photon measurement, or a more effective, coherent photon protocol that has comparatively less fidelity.

To tackle such a dilemma, in this chapter we introduce a robust and cavity-free distant entanglement protocol using resonance fluorescence. By coupling the laser photons with the qubits in a Mach-Zehnder type interferometer, the outgoing fluorescence signals can have very different number of photons depending on the entanglement status of the qubits. We can thereby achieve entanglement between these distant qubits through the postselection of the detected many-photon states. This multiphoton method does not require any single-photon detector, or sensitive phase measurement, thus have a higher rate of success without sacrificing the entanglement fidelity. Fluorescence is highly effective for its detection [15] and for

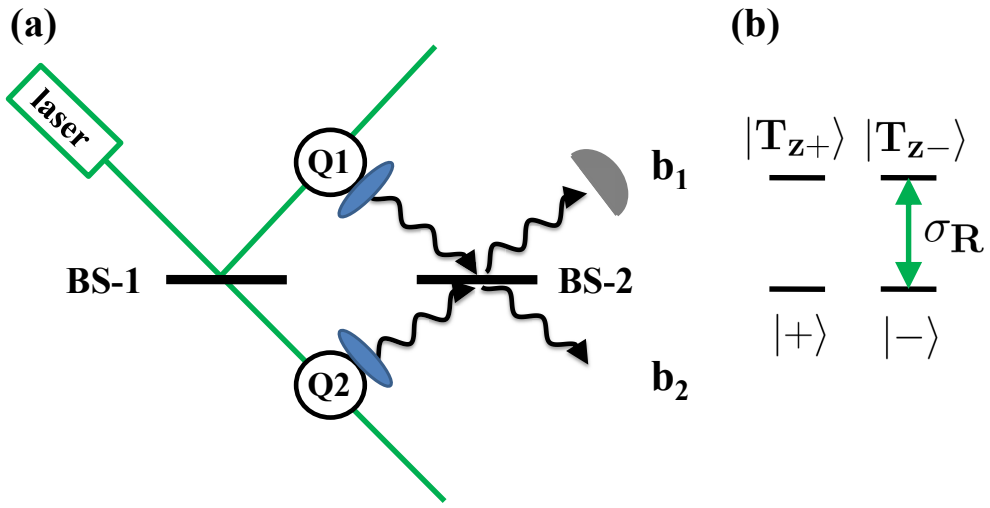

Figure 4.1: (a) Schematic for the entanglement of distant qubits based on multiphoton scattering. Two circularly polarized laser modes split from a laser by the first beam splitter (BS-1) are directed to excite two qubit systems at resonance. The scattered fluorescence signals are collected to interfere at the second beam splitter. Due to the optical selection rule, the fluorescence signal serves as a fingerprint of the state of the electronic spin such that its detection at b_1 would postselectively project the two qubits state to an entangled state. (b) provides an example of energy levels in the QD qubit system, where the laser only selectively couples the $-3/2$ trion state $|T_{z-}\rangle$ and the $-1/2$ spin state $|-\rangle$.

this reason, has been used in the proposal of entanglement distribution in quantum repeaters once entanglement is created [16]. Our scheme takes the same advantage of fluorescence and only involves the detection and distinguishabilty of the many-photon fluorescence signals, feasible using current experimental technology.

4.2 The entanglement mechanism

Fig. 4.1(a) shows our setup to entangle two distant qubits. For illustrative purpose, we consider the singly charged quantum dot (QD) as our qubit systems [17, 18], where each dot consists of four energy levels as shown in Fig. 4.1(b). Direct generalization to other qubit systems, such as the diamond nitrogen-vacancy center, is straightforward. The two electronic spin states $|\pm\rangle$ form the qubit states,

while only the $|-\rangle$ state would be optically coupled to the spin $-3/2$ trion state $|T_{z-}\rangle$ through the right-handed circularly polarized laser due to the selection rules. In our scheme, we first split the circularly polarized laser pulse by a polarization-independent beam splitter (BS-1) [19], and then direct the outgoing beams to drive the two distant qubit systems. The resonance fluorescence signals scattered from the qubit systems are collected, say by optical lenses and then pass through another beam splitter (BS-2). Owing to the state dependence of the resonance fluorescence, the scattered multiphoton state is entangled with the entire qubit system. Consider each qubit is initially prepared in the state $|x+\rangle = (|+\rangle + |-\rangle)/\sqrt{2}$, the qubit-photon wavefunction after the second beam splitter is given by:

$$\frac{U_{\rm BS}}{2}\Big[\ \ |++\rangle\,|0;0\rangle + |-+\rangle\,|\beta;0\rangle + |+-\rangle\,|0;-i\beta\rangle + |--\rangle\,|\beta;-i\beta\rangle\ \ \Big], \qquad (4.1)$$

where $U_{\rm BS}$ represents the beam splitter transformation and $|\beta;-i\beta\rangle$ denotes the multiphoton state scattered from the qubits. We note that the resonance fluorescence photon state is not a coherent Glauber state and the effect of $U_{\rm BS}$ on it is not just a simple photon amplitude transformation. We shall see below that the multiphoton states associated with $|+-\rangle$ and $|-+\rangle$ share the same mean number of photons, but are macroscopically different from the remaining two states. In consequence, a detection of the final photon state would project the qubit system to an entangled state with a probability of 1/2. Such a postselection scheme shares the same high entanglement fidelity as in the single-photon protocol, but exponentially boosts up the entanglement efficiency as only multiphoton measurement is involved.

The many-photon resonance fluorescence establishes a robust entanglement between the photons and the qubits. The photon dynamics is governed by:

$$a_{s,k}(t) = e^{-i\omega_k t}a_{s,k}(0) - ig_k\int_0^t dt'\sigma_{s,-}(t')e^{-i\omega_k(t-t')}, \qquad (4.2)$$

where ω_k and g_k are respectively the photon frequency and dipole-electric coupling, $\sigma_- = |-\rangle\langle T_{z-}|$, and $s = 1, 2$ denotes the upper or lower channel of the interferometer. The first term provides the laser input route, while the second

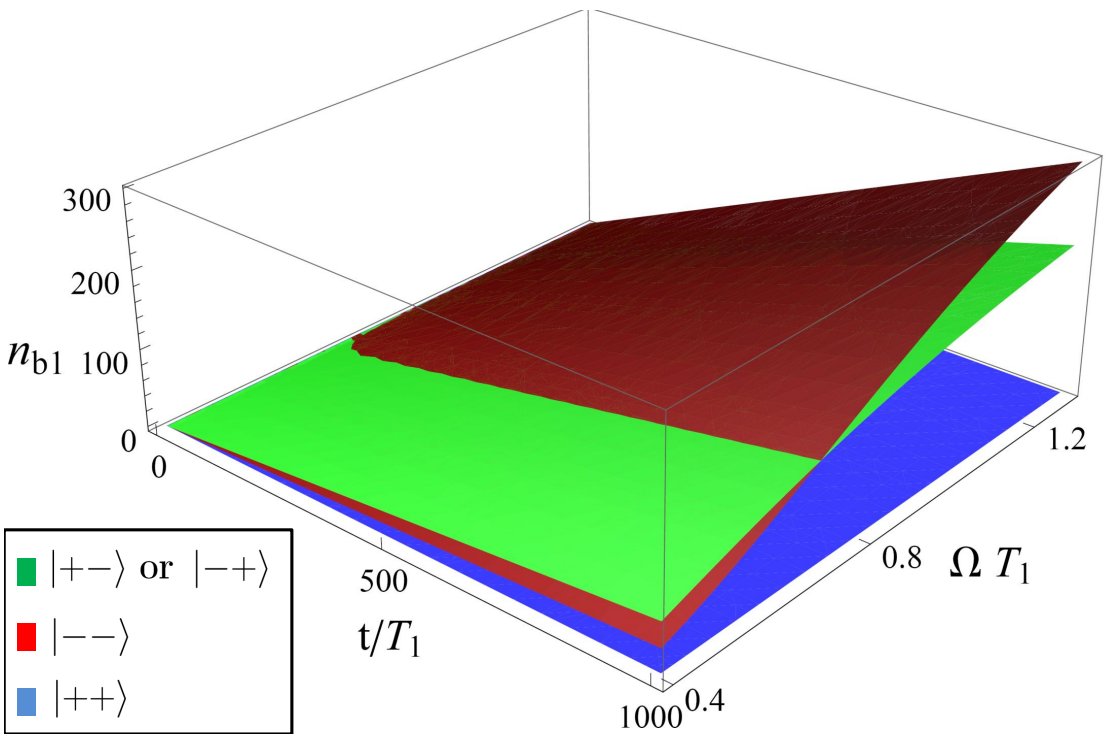

Figure 4.2: Time and Rabi frequency dependences of the average number of photon detected at b_1 for $\eta = 1$. Apart from the signal corresponding to the $|++\rangle$ state, the fluorescence signals increase linearly with time when $t \gg T_1$ and are distinct, except in the field regime $\Omega T_1 \sim 0.7$.

term corresponds to the scattered photons through resonance fluorescence and is further transformed by the second beam splitter. For our process, the entanglement is heralded by the photons arriving at detector b_1, different from the double click scenario in the single-photon scheme.

The state-selective number of photons being detected at b_1 can be evaluated by the optical Bloch equation [20] as:

$$\begin{aligned} n_{b_1;++}(t) &= 0, \\ n_{b_1;+-(-+)}(t) &= \frac{\eta}{4T_1}\int_0^t dt' \left\langle \sigma_{2(1),z}(t') + 1 \right\rangle, \\ n_{b_1;--}(t) &= \frac{\eta}{2T_1}\sum_{s,s'}\int_0^t dt'(-1)^{s+s'} \left\langle \sigma_{s,+}(t')\sigma_{s',-}(t') \right\rangle, \end{aligned} \tag{4.3}$$

Here, T_1 is the relaxation time for the transition $|-\rangle \leftrightarrow |T_{z-}\rangle$, and η is the efficiency

of both photon collection and detection. Fig. 4.2 plots the maximum number of detected photons (i.e. $\eta = 1$) as a function of time and Rabi frequency, Ω of the qubit. Large numbers of photons are generated conditioned on the qubit states and increase linearly with time when $t \gg T_1$. The distinguishability between $n_{b_1;+-(-+)}$ and the other two numbers of photons in most of the region allows a probabilistic entanglement generation by postselection with an ideal probability of 1/2, compared to 1/4 in the single-photon protocol. We note that the dark transitions due to the hole mixing in QD system [21], which would lead to an estimated 1% of fluorescence photons, are negligible in this many-photon entanglement scheme.

The field dependence of the detected photons divides the entanglement scheme into two regimes. For low driving field ($\Omega T_1 \ll 0.7$), the entangled state has fluorescence photon number being much larger than that of the unentangled one. This resembles a Glauber state situation. If we approximate the fluorescence photon state $|\beta\rangle$ in Eq. (4.1) as the Glauber state, then the second beam splitter will simply transform $|\beta; 0\rangle$ to $\left|i\beta/\sqrt{2}; \beta/\sqrt{2}\right\rangle$ and $|\beta; -i\beta\rangle$ to $\left|0; \sqrt{2}\beta\right\rangle$, so that no photon would be available in the detector b_1 for the $|--\rangle$ state. The fact that there is a finite but small signal in $n_{b_1;--}$ reflects the non-Glauber nature of the fluorescence signal. On the other hand, for large Rabi frequency ($\Omega T_1 > 0.7$), $n_{b_1;--}$ exceeds $n_{b_1;\pm\mp}$ and the Glauber characteristics of the photon state entirely disappears. In both regimes, entanglement generation is feasible, though the high field region would be more effective due to its larger number of fluorescence photons.

4.3 Noise analysis

We now analyze the noise of our entanglement scheme. Unlike the single-photon protocol whose fidelity is limited by dark counts in the experiment, our multiphoton entanglement approach is not sensitive to the background noise, but relies on a clear distinction between large fluorescence signals. The study of photon statistic in resonance fluorescence has been well studied since Mandel [22] and has been verified in atomic experiments [24]. We make use of the same approach by

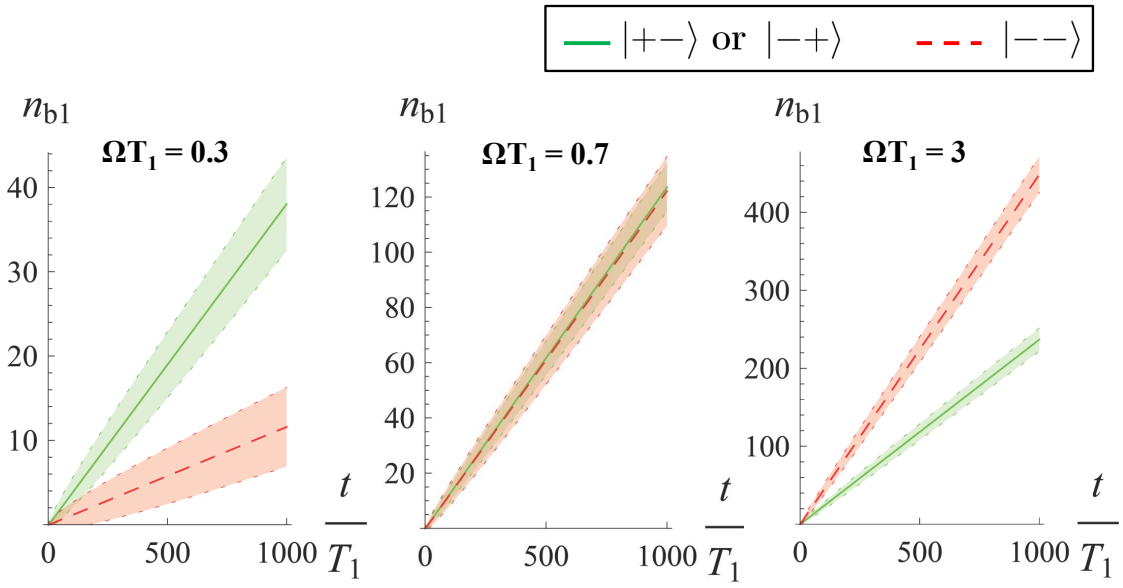

Figure 4.3: Fluctuations in the number of detected fluorescence photons for various field strengths. Shaded areas refer to the region of $n_{b_1} \pm \Delta n_{b_1}$. Signals corresponding to entangled and unentangled states can be easily separated with a fidelity larger than 95% in both the low and high field domains.

Mandel in our entanglement process and compute the fluctuations in the number of detected photons by [22]:

$$\Delta n_{b_1}(t)^2 = n_{b_1}(t) + \frac{\eta^2}{2T_1^2} \sum_{s_1,s_2,s_3,s_4} \int_0^t dt_2 \int_0^{t_2} dt_1 \times (-1)^{s_1+s_2+s_3+s_4} \langle \sigma_{s_1,+}(t_1)\sigma_{s_2,+}(t_2)\sigma_{s_3,-}(t_2)\sigma_{s4,-}(t_1)\rangle \,. \tag{4.4}$$

The four-point correlation functions can be evaluated using the quantum regression theorem [20], being applicable for our qubit system.

Fig. 4.3 illustrates how the noise of the maximally detected fluorescence photons depends on the qubit state. It is clear that the many-photon fluorescence signals are differentiable in both the low and high field regimes, even in the presence of photon number fluctuation. A long time operation is necessary for increasing the number of fluorescence photons as well as suppressing the signal to noise ratio.

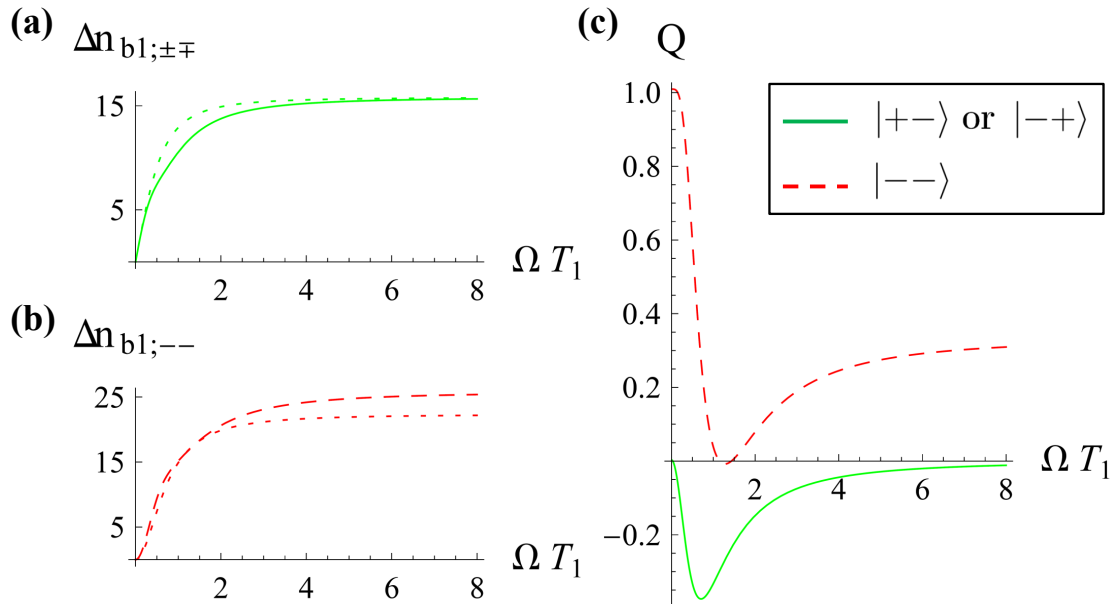

Figure 4.4: (a) and (b) show the field dependence of photon fluctuations for entangled and unentangled states at $t/T_1 = 10^3$. Dotted lines represent poissonian noises. $\Delta n_{b_1;\pm\mp}$ and $\Delta n_{b_1;--}$ are sub-poissonian and super-poissonian respectively. (c) provides the corresponding Mandel parameters. The super-poissonian statistics is not significant enough to destroy the distinguishability of fluorescence signals.

High field is preferred for the same reason. The fluorescence signal saturates at $\Omega T_1 \sim 3$ and approaches the asymptotic values $n_{b_1;\pm\mp}(t) \to t/4T_1$ and $n_{b_1;--}(t) \to t/2T_1$ at larger field strength.

Fig. 4.4 details the field dependence of the noise statistic of photons for the entangled and unentangled states for $\eta = 1$. At large time ($t/T_1 = 10^3$), the photon signal corresponding to the entangled state demonstrates a sub-poissonian statistics as shown in Fig. 4.4(a). This result is just the same as that of the standard resonance fluorescence, since the entangled state only consists of fluorescence photon from either one of the qubit. By contrast, the photons associated with the unentangled state $|--\rangle$ exhibits super-poissonian behavior in the entire field domain. Fig. 4.4(c) shows that the Mandel parameter, $Q = (\Delta n_{b_1})^2/n_{b_1} - 1$, for the unentangled state can be as large as 1 in the low field regime and approaches to the asymptotic value of 1/3 in the large field limit, in agreement with the non-Glauber character of the photon state described above. We remark that

the Mandel parameter is limited by the photon collection and detection efficiency, so that $|Q| \sim \eta \ll 1$ and the measured photon statistics will be very close to poissonian in the realistic experimental situation.

4.4 Efficiency study

An important aspect of all the entanglement mechanism is the average entanglement rate. The low efficiency of the entanglement protocol using single-photon detection severely limits the rate of each successful operation. For instance, in the existing trapped ions experiment [5], the success probability is as low as $\sim 2.2 \times 10^{-8}$, leading to an average entanglement time around 600 s, longer than the decoherence time of the trapped ion qubit. This posts a dramatic restriction to the scalability of the corresponding qubit systems. While experimental technique is advancing to increase the efficiency of single-photon collection and detection, our entanglement generation scheme based on the many-photon resonance fluorescence signal does not possess such a problem and can have a success probability close to unity. We discuss our entanglement rate in the following. Our entanglement scheme depends on the distinction of fluorescence signals corresponding to entangled and unentangled states (Fig. 4.3). In the large field region ($\Omega T_1 > 3$), these two signals are already well separated with a confidence level (or fidelity) being more than 95%, when $\eta \times t/T_1 \approx 100$. In other words, we can easily reach the ideal success probability (i.e. 1/2) using a "long" operational time, depending on η. Taking the same trapped ion example, the collection and detection efficiencies are 2% and 15% respectively, so that $\eta = 3 \times 10^{-3}$. This corresponds to our average entanglement time being $\sim 6.7 \times 10^4$ $T_1 \approx 530$ μs (T_1 being the spontaneous emission time for the $^2P_{1/2}$ to $^2S_{1/2}$ transition in the trapped ion qubit), which is six orders less than that of the single-photon protocol and more importantly, much shorter than the decoherence time of the trapped ion system. Similarly, for the nitrogen-vacancy center qubit system with a typical spontaneous emission time ~ 10 ns [23], an average entanglement time of several hundred microseconds can be achieved with the same order of η, and is below its millisecond coherence time

scale.

The same is true for the QD qubits in spite of the relatively less decoherence time. In the singly charged QD system, the upper trion state roughly has the relaxation time $T_1 \approx 0.1$ ns [17]. Taking realistic collection (6.7%) and detection (15%) efficiencies in the resonance fluorescence experiments [24], our multiphoton entanglement scheme has an average entanglement time ~ 2 μs, which is within the electron coherence time achieved in the spin echo experiment of a single QD [25]. Such a coherence time scale can also be reached by using the coherent dark-state spectroscopy [26, 27]. This many-photon entanglement scheme has to be contrasted with the single-photon protocol that would instead result in an estimated time to entangle two distant QDs to be of the order of ten milliseconds on average, based on the existing physical parameters. In other words, unlike the single-photon entanglement protocol that requires a sharp improvement in the experimental performance of single-photon measurements, the multiphoton approach is more suitable for a scalable qubit entanglement under the current experimental condition.

Another advantage of this multiphoton entanglement method is its insensitivity to the mismatch of the optical characters of the two qubits. The single-photon protocol is based on the Hong-Ou-Mandel interferometry that relies on a good frequency matching of the spontaneously emitted photons from two different qubits. Slight discrepancy in the resonant frequency of qubits in QD system would lead to a wrong double click signal even though the qubits are not entangled, thereby depress the overall entanglement fidelity in the single-photon mechanism. Our scheme is more robust in this aspect. Consider two qubit systems having different resonant frequencies (ω_0, ω_0'), Rabi frequencies (Ω, Ω') and relaxation times (T_1, T_1'), but the same photon collection and detection efficiency. According to Eq. (4.3), the large field behaviors of the fluorescence signals in this situation are that $n_{b_1;++} = 0$, $n_{b_1;+-} \approx \eta\ t/4T_1$, $n_{b_1;-+} \approx \eta\ t/4T_1'$ and $n_{b_1;--} \approx (\eta\ t/4)(1/T_1 + 1/T_1')$. This means that our entanglement method is insensitive to frequency mismatch, and the $|--\rangle$ state is still differentiable from the other states for a moderate difference in T_1. In order to maintain the coherence

of the entangled state, the difference in the corresponding fluorescence signals cannot be too large, i.e. $|n_{b_1;+-} - n_{b_1;-+}| < \Delta n_{b_1;\pm\mp}$. For $\eta t/T_1 \approx 100$, this roughly corresponds to a ten percent relative discrepancy in the relaxation rate. In this regime, a high rate and fidelity entanglement is still feasible.

4.5 Summary

In summary, we have introduced a new entanglement generation scheme using postselection of coherent multiphoton signals. It improves on the single-photon protocols by increasing the success probability and the average entanglement rate by several orders of magnitude, while maintaining the high fidelity of entanglement. Without significant enhancement in single-photon measurement efficiency, nor surrounding the qubit by an optical cavity, this proposed multiphoton protocol already allows an average entanglement of two distant qubits before their decoherence based on current experimental technologies, while experimental improvements would further reduce the operational duration. We believe this would open a new direction in the design of hybrid multiphoton-qubit network in quantum information processing.

4.6 Acknowledgments

This research was supported by the U.S. Army Research Office MURI award W911NF0910406 and by NSF grant PHY-1104446. C. K. Chan thanks Bo Sun for a useful discussion.

The text in chapter 4, in part, is a reprint of the material as it appears in Ching-Kit Chan and L. J. Sham, "Robust distant-entanglement generation using coherent multiphoton scattering", under review of Physical Review Letter. The dissertation author was the first author of the paper and the co-author in this publication directed, supervised, and co-worked on the research which forms the basis of this chapter.

Bibliography

[1] L.-M. Duan, M. D. Lukin, J. I. Cirac and P. Zoller, "Long distance quantum communication with atomic ensembles and linear optics", Nature **414**, 413 (2001).

[2] L. I. Childress, J. M. Taylor, A. S. Sørensen and M. D. Lukin, "Fault-tolerant quantum repeaters with minimal physical resources and implementations based on single-photon emitters", Phys. Rev. A. **72**, 052330 (2005).

[3] L.-M. Duan, M. J. Madsen, D. L. Moehring, P. Maunz, R. N. Kohn, Jr., and C. Monroe, "Probabilistic quantum gates between remote atoms through interference of optical frequency qubits", Phys. Rev. A. **73**, 062324 (2006).

[4] E. Waks and C. Monroe, "Protocol for hybrid entanglement between a trapped atom and a quantum dot", Phys. Rev. A **80**, 062330 (2009).

[5] L.-M. Duan and C. Monroe, "Quantum networks with trapped ions", Rev. Mod. Phys. **82**, 1209 (2010).

[6] D. L. Moehring, P. Maunz, S. Olmschenk, K. C. Younge, D. N. Matsukevich, L.-M. Duan and C. Monroe, "Entanglement of single atom quantum bits at a distance", Nature **449**, 68 (2007).

[7] P. Maunz, S. Olmschenk, D. Hayes, D. N. Matsukevich, L.-M. Duan and C. Monroe, "Heralded quantum gate between remote quantum memories", Phys. Rev. Lett. **102**, 250502 (2009).

[8] S. Olmschenk, D. N. Matsukevich, P. Maunz, D. Hayes, L.-M. Duan and C. Monroe, "Quantum teleportation between distant matter qubits", Science **323**, 486 (2009).

[9] G. Shu, N. Kurz, M. R. Dietrich and B. B. Blinov, "Efficient fluorescence collection from trapped ions with an integrated spherical mirror", Phys. Rev. A **81**, 042321 (2010).

[10] D. Englund, B. Shields, K. Rivoire, F. Hatami, J. Vuckovic, H. Park and M. D. Lukin, "Deterministic coupling of a single NV center to a photonic crystal cavity", Nano Lett. **10**, 3922 (2010).

[11] D. Le Sage, L. M. Pham, N. Bar-Gill, C. Belthangady, M. D. Lukin, A. Yacoby and R. L. Walsworth, "Efficient photon detection from color centers in a diamond optical waveguide", e-prints arXiv:1201.0674 (2012).

[12] P. van Loock, T. D. Ladd, K. Sanaka, F. Yamaguchi, K. Nemoto, W. J. Munro and Y. Yamamoto, "Hybrid quantum repeater using bright coherent light", Phys. Rev. Lett. **96**, 240501 (2006).

[13] P. van Loock, N. Lutkenhaus, W. J. Munro and K. Nemoto, "Quantum repeaters using coherent state communication", Phys. Rev. A **78**, 062319 (2008).

[14] Y. P. Huang and M. G. Moore, "On demand generation of entanglement of atomic qubits via optical interferometry", Phys. Rev. A **77**, 032349 (2008).

[15] A. H. Myerson, D. J. Szwer, S. C. Webster, D. T. C. Allcock, M. J. Curtis, G. Imreh, J. A. Sherman, D. N. Stacey, A. M. Steane and D. M. Lucas, "High fidelity readout of trapped ion qubits", Phys. Rev. Lett. **100**, 200502 (2008).

[16] J. B. Brask, L. Jiang, A. V. Gorshkov, V. Vuletic, A. S. Sørensen and M. D. Lukin, "Fast entanglement distribution with atomic ensembles and fluorescent detection", Phys. Rev. A **81**, 020303 (2010).

[17] X. Xu, Y. Wu, B. Sun, Q. Huang, J. Cheng, D. G. Steel, A. S. Bracker, D. Gammon, C. Emary and L. J. Sham, "Fast Spin State Initialization in a Singly Charged InAs-GaAs Quantum Dot by Optical Cooling", Phys. Rev. Lett. **99**, 097401 (2007).

[18] X. Xu, B. Sun, P. R. Berman, D. G. Steel, A. S. Bracker, D. Gammon and L. J. Sham, "Coherent Population Trapping of an Electron Spin in a Single Negatively Charged Quantum Dot", Nature Physics **4**, 692 (2008).

[19] See for example, X.-S. Ma, S. Zotter, N. Tetik, A. Qarry, T. Jennewein and A. Zeilinger, "A high speed tunable beam splitter for feed forward photonic quantum information processing", Optics Express **19**, 22723 (2011).

[20] See for example, M. O. Scully and M. S. Zubairy, *Quantum Optics* (Cambridge Univ. Press, Cambridge, 1997).

[21] R.-B. Liu, W. Yao and L. J. Sham, "Quantum computing by optical control of electron spins", Advances in Physics **59**, 703 (2010).

[22] L. Mandel, "Subpoissonian photon statistics in resonance fluorescence", Optics Lett. **4**, 205 (1979).

[23] E. Togan, Y. Chu, A. S. Trifonov, L. Jiang, J. Maze, L. Childress, M. V. G. Dutt, A. S. Sørensen, P. R. Hemmer, A. S. Zibrov1 and M. D. Lukin, "Quantum entanglement between an optical photon and a solid state spin qubit", Nature **466**, 730 (2010).

[24] R. Short and L. Mandel, "Observation of subpoissonian photon statistics", Phys. Rev. Lett. **51**, 384 (1983).

[25] D. Press, K. De Greve1, P. L. McMahon, T. D. Ladd, B. Friess, C. Schneider, M. Kamp, S. Hofling, A. Forchel and Y. Yamamoto, "Ultrafast optical sin echo in a single quantum dot", Nature Photonics **4**, 367 (2010).

[26] X. Xu, W. Yao, B. Sun, D. G. Steel, A. S. Bracker, D. Gammon and L. J. Sham, "Optically controlled locking of the nuclear field via coherent dark-state spectroscopy", Nature **459**, 1105 (2009).

[27] B. Sun, W. Yao, X. Xu, A. S. Bracker, D. Gammon, L. J. Sham and D. G. Steel, "Persistent optical nuclear spin narrowing in a singly charged InAs quantum dot", J. Opt. Soc. Am. B **29**, A119 (2012).

Chapter 5

Conclusion and outlook

In this chapter, we summarize the main results of this dissertation. Relevant future directions will also be discussed.

Owing to the need of a high accuracy standard in quantum technology, we have reexamined existing open quantum system theories and have developed a new theoretical framework to evaluate the interaction dynamics of a quantum system under a quantum photonic control and photonic environment. We have demonstrated how this approach is particularly suitable for solving the open quantum system problem. This new theoretical direction goes beyond the traditional Master equation paradigm in several ways. It is precise, has a well-controlled error bound and is suitable for calculating the quantum decoherence and quantum noise in the time scale of a fast quantum operation versus slow decoherence, which is relevant to the quantum information technology. This technique does not require any a priori stochastic assumption and is applicable to both Markovian and non-Markovian environments. It is not restricted to deal with semiclassical photonic control and is applicable to a general photonic control state. All quantum correlations among the system, the quantum control and the environment are maintained under this new methodology.

The diagrammatic approach developed so far can have a lot of possible extension. One important direction is to go beyond the small decoherence time regime. The long time behavior of an open quantum system becomes important when we attempt to prolong the decoherence time, say by the dynamical decoupling

scheme, where a sequence of pre-designed photon pulses are applied to the system, in a way to try to effectively decouple the system from the environment and extend the decoherence time. In this scenario, the time regime longer than the intrinsic decoherence time scale would be of interest. While the long time behavior of the open quantum system is a challenging question to all open quantum system theories, the diagrammatic approach could provide a better way to tackle this problem by performing partial summations of the long time diagrams, similar to the Bethe-Salpeter approximation well-known in condensed matter physics and high energy physics. The advantage of using diagram is that an error bound can always be well defined.

Another interesting generalization of the current diagrammatic theory is to apply it to systems with a spin environment. This is important to quantum dot and diamond nitrogen vacancy center qubit systems, as their decoherence mechanisms are mainly due to the surrounding nuclear spin environment. For this spin bath problem, a possible application of the diagrammatic approach is to first transform the nuclear spin into either Schwinger boson or Holstein-Primakoff boson, so that the Wick's expansion can be easily applied. We believe this novel approach can provide some new insights to the spin bath problem.

On the other hand, we have also made use of the photonic environment to engineer quantum entanglement between distinct qubit systems. The driven qubits emit large and different fluorescence photons that allow the distinguishability of entangled and unentangled qubit states. Therefore, based on the detection of fluorescence signals, one can postselectively project the qubit states to the entanlged states, even though they have no local interaction. This entanglement generation scheme based on multiphoton scattering shows a remarkable improvement in entanglement efficiency, compared to the single photon approach. An interesting extension of this work is to employ a non-Markovian photonic environment. One possible scenario is the Jaynes-Cummings qubit-photon system, where interesting phenomena, like the collapse and revival of the qubit, can occur due to the non-Markovian nature of the environment. It will be interesting to see whether we can utilize this effect for entanglement generation.